

# Non-LTE line formation for Pr II and Pr III in A and Ap stars

L. Mashonkina<sup>1,2</sup>, T. Ryabchikova<sup>2,3</sup>, A. Ryabtsev<sup>4</sup>, and R. Kildiyarova<sup>4</sup>

<sup>1</sup> Institut für Astronomie und Astrophysik der Universität München, Scheinerstr. 1, 81679 München, Germany  
e-mail: lyuda@usm.lmu.de

<sup>2</sup> Institute of Astronomy, Russian Academy of Sciences, Pyatnitskaya 48, 119017 Moscow, Russia  
e-mail: lima@inasan.ru

<sup>3</sup> Institute for Astronomy, University of Vienna, Türkenschanzstrasse 17, A-1180 Vienna, Austria

<sup>4</sup> Institute of Spectroscopy, Russian Academy of Sciences, 142190, Troitsk, Moscow region, Russia

Received / Accepted

## ABSTRACT

**Aims.** Non-local thermodynamical equilibrium (non-LTE) line formation for singly-ionized and doubly-ionized praseodymium is considered through a range of effective temperatures between 7250 K and 9500 K. We evaluate the influence of departures from LTE on Pr abundance determinations and determine a distribution of the Pr abundance in the atmosphere of the roAp star HD 24712 from non-LTE analysis of the Pr II and Pr III lines.

**Methods.** A comprehensive model atom for Pr II/III is presented based on the measured and the predicted energy levels, in total, 6708 levels of Pr II and Pr III and the ground state of Pr IV. Calculations of the Pr II energy levels and oscillator strengths for the transitions in Pr II and Pr III are described.

**Results.** The dependence of non-LTE effects on the atmospheric parameters is discussed. At  $T_{\text{eff}} \geq 8000$  K departures from LTE lead to overionization of Pr II and, therefore, to systematically depleted total absorption in the line and positive abundance corrections. At the lower temperatures, different lines of Pr II may be either weakened or amplified depending on the line strength. The non-LTE effects strengthen the Pr III lines and lead to negative abundance corrections. Non-LTE corrections grow with effective temperature for the Pr II lines, and, in contrast, they decline for the Pr III lines. The Pr II/III model atom is applied to determine the Pr abundance in the atmosphere of the roAp star HD 24712 from the lines of two ionization stages. In the chemically uniform atmosphere with  $[\text{Pr}/\text{H}] = 3$ , the departures from LTE may explain only small part (approximately 0.3 dex) of the difference between the LTE abundances derived from the Pr II and Pr III lines ( $\approx 2$  dex). We find that the lines of both ionization stages are described for the vertical distribution of the praseodymium where the Pr enriched layer with  $[\text{Pr}/\text{H}] \geq 4$  exists in the outer atmosphere at  $\log \tau_{5000} < -4$ . The departures from LTE for Pr II/III are strong in the stratified atmosphere and have the opposite sign for the Pr II and Pr III lines. The praseodymium stratification analysis of roAp stars has to be performed based on non-LTE line formation. Using the revised partition function of Pr II and experimental transition probabilities, we determine the solar non-LTE abundance of Pr as  $\log (\text{Pr}/\text{H})_{\odot} = -11.15 \pm 0.08$ .

**Key words.** Atomic data – Atomic processes – Line: formation – Stars: atmospheres – Stars: chemically peculiar – Stars: individual: HD 24712

## 1. Introduction

Classical LTE analysis finds a great violation of the ionization equilibrium between the second and the first ions of the rare-earth elements (REE) in rapidly oscillating chemically peculiar (roAp) stars (Cowley & Bord 1998, Cowley et al. 2000, Gelbmann et al. 2000, Ryabchikova et al. 2000, Kochukhov 2003, Ryabchikova et al. 2001). For the sample of 26 stars, Ryabchikova et al. (2001) show that a discrepancy between the abundances derived from the lines of singly ionized and doubly ionized atoms of neodymium and praseodymium typically exceeds 1.5 dex in roAp stars, while it is substantially smaller if exists in non-pulsating Ap stars (see also Kato 2003; Ryabchikova et al. 2006 for hotter Ap stars HD 170973 and HD 144897). This rules out errors in the oscillator strengths as a possible reason for the abundance difference observed in roAp stars.

In our previous paper (Mashonkina et al. 2005), we investigate the Nd II and Nd III spectra in two roAp stars,  $\gamma$  Equ and HD 24712, based on non-local thermodynamic equilibrium (non-LTE) line formation and show that the non-LTE effects may explain only 0.5 dex of the difference between the LTE abun-

dances derived from the Nd II and Nd III lines and not the 1.5 – 2.0 dex observed in these stars. Mashonkina et al. come back, therefore, to the assumption of Ryabchikova et al. (2002) that the Nd anomaly observed in  $\gamma$  Equ is caused by a stratified Nd distribution with the accumulation of the element in the uppermost atmospheric layers, above  $\log \tau_{5000} = -8$  according to the LTE analysis. It was found that the non-LTE effects for the Nd II and Nd III lines are very strong in the stratified atmosphere, and they result in significant shifting the Nd enriched layer downward compared to the location determined in the LTE analysis. The required Nd overabundance in the layer is  $[\text{Nd}/\text{H}] = 4$  at  $\log \tau_{5000} < -3.5$  for  $\gamma$  Equ and  $[\text{Nd}/\text{H}] = 4.5$  at  $\log \tau_{5000} < -4.5$  for HD 24712.

The present paper continues to investigate the rare-earth elements in stellar atmospheres based on the non-LTE line formation and is devoted to the praseodymium. We study the statistical equilibrium (SE) of singly ionized and doubly ionized praseodymium, Pr II and Pr III, through a range of effective temperatures between 7250 K and 9500 K, evaluate the influence of departures from LTE on Pr abundance determinations in the Sun, A and Ap type stars, consider the non-LTE effects for Pr II/III in the atmosphere with non-uniform vertical distribution of Pr, and

Send offprint requests to: L. Mashonkina

finally determine empirically a stratification of Pr in the atmosphere of the roAp star HD 24712 from the non-LTE analysis of the Pr II and Pr III lines.

The paper is organized as follows. In Sect. 2, an extensive model atom for Pr II/III is introduced and theoretical calculations of the Pr II atomic structure and transition probabilities for Pr II and Pr III are presented. The programs and atmospheric models used in the line formation calculations are described in Sect. 3. Section 4 investigates the departures from LTE for Pr II/III in the model atmospheres with homogeneous and stratified distribution of Pr. The non-LTE abundance corrections for the selected lines of Pr III and Pr II are given there depending on effective temperature. The solar Pr abundance is revised in Sect. 5 based on the improved partition function of Pr II. In Sect. 6, we determine the Pr abundance distribution in the atmosphere of the roAp star HD 24712 from the non-LTE analysis of the Pr II and Pr III lines and discuss the influence of the uncertainties of atomic parameters on non-LTE modelling and final results. Our conclusions and recommendations are given in Sect. 7.

## 2. Model atom of Pr II-Pr III

Model atom provides the necessary atomic input data to specify the SE equations and the opacities/emissivities for radiative transfer calculations.

### 2.1. Energy levels

The lower levels in singly ionized Pr belong to the  $4f^3 6s$  configuration with the  $(^4I)^3I$  ground term. Laboratory measurements (Ginibre 1989a, 1989b, Furman et al. 2001, Ivarsson et al. 2001) give 330 energy levels of Pr II with an excitation energy  $E_{\text{exc}} \leq 5.3$  eV. Most known levels belong to singlet, triplet, and quintet terms of the  $4f^3 nl$  ( $nl = 6s, 5d, 6p$ ) and  $4f^2 5d nl$  ( $nl = 5d, 6s, 6p$ ) electronic configurations. For some of the known energy levels, only the total angular momentum and assignment to an electronic configuration were given. The highest known levels of Pr II are separated by more than 5 eV from the ground state of Pr III. The calculations with the Cowan (1981) code show that even below 5.3 eV there are many unidentified energy levels. With such an incomplete term system we cannot get a realistic statistical equilibrium of the atom.

For the present study, we calculate the energy levels of Pr II using the Cowan code (Cowan 1981). The measured levels of the odd  $4f^3 6s + 4f^3 5d + 4f^2 5d 6p$  configurations have been fitted taking into account the interactions with the  $4f^2 6s 6p$ ,  $4f 5d^3$ ,  $4f 5d^2 6s$ , and  $4f 5d 6s^2$  configurations. The  $4f^2 5d^2$ ,  $4f^2 5d 6s$ ,  $4f^2 6s^2$ ,  $4f^3 6p$ ,  $4f^4$ ,  $4f^2 6p^2$ , and  $4f 5d^2 6p$  configurations are included in the fitted matrix of the even system. The fitting results in a standard deviation of the calculated from experimental levels of  $86 \text{ cm}^{-1}$  for 129 odd and  $72 \text{ cm}^{-1}$  for 201 even levels. To get highly excited levels the energy structures of the even  $4f^3(7p-9p)$  and  $4f^3(5f-6f)$  configurations and the odd  $4f^3(7s-9s)$ ,  $4f^3(6d-8d)$ ,  $4f^3 5g$ , and  $4f^2 5d 5f$  configurations are calculated. In all unknown configurations, the average energies where Brewer (1971) predictions are absent and the energy parameters of the  $4f^2$  and  $4f^3$  cores are scaled similarly to the known configurations, the other parameters being scaled by a factor 0.75 with respect to the corresponding Hartree - Fock values. As a result, a nearly complete set of the levels below  $70000 \text{ cm}^{-1}$  (8.7 eV) has been obtained consisting of 3938 energies. All the known levels and the predicted levels with  $E_{\text{exc}} \leq 10.04$  eV, in total 6539 levels of Pr II, are used to construct the model atom. They are shown in Figs. 1 and 2 (Online only) for

**Table 1.** Partition functions for Pr II and Pr III.

| Temperature<br>(K) | Pr II          |            | Pr III<br>this study |
|--------------------|----------------|------------|----------------------|
|                    | Ginibre (1989) | this study |                      |
| 3000               | 55             | 58         | 22                   |
| 4000               | 91             | 101        | 28                   |
| 5000               | 138            | 166        | 34                   |
| 6000               | 192            | 251        | 43                   |
| 7000               | 252            | 356        | 54                   |
| 8000               | 315            | 478        | 66                   |
| 9000               | 380            | 617        | 81                   |
| 10000              | 446            | 770        | 97                   |
| 11000              | 511            | 937        | 114                  |
| 12000              | 576            | 1117       | 132                  |
| 13000              | 639            | 1309       | 151                  |
| 14000              | 701            | 1514       | 170                  |
| 15000              | 762            | 1732       | 190                  |
| 16000              | 820            | 1962       | 211                  |
| 17000              | 878            | 2205       | 231                  |
| 18000              | 933            | 2460       | 252                  |
| 19000              | 986            | 2727       | 273                  |
| 20000              | 1038           | 3007       | 293                  |

the even and odd levels, correspondingly. The calculated high excitation levels provide the close collisional coupling of Pr II to the continuum electron reservoir.

It is worth noting that the calculations lead to a significantly larger partition function of Pr II compared to that based on the laboratory levels only. This is illustrated in Table 1, where the partition function of Pr II is calculated by its definition for a temperature range 3000 K – 20000 K using the measured energy levels from Ginibre (1989a, 1989b) and using the levels predicted in this study. In Sect. 5, we calculate the effect of the revised partition function on the Pr abundance determined from the solar Pr II lines.

For Pr III, the laboratory measurements resulted in 593 energy levels (Martin et al. 1978, Palmeri et al. 2000) with an excitation energy up to 17.5 eV. In the range of stellar parameters we are concerned with, there is no need to include the highly excited levels of Pr III in the model atom. They play a minor role in population and depopulation of Pr III, because the next ionization stage Pr IV represents a negligible fraction of Pr abundance. We use, therefore, the levels of the odd  $4f^3$  and the even  $4f^2 5d$  and  $4f^2 6s$  electronic configurations with  $E_{\text{exc}} \leq 6.7$  eV. The term structure is shown in Fig. 3 (Online only). The contribution of the Pr III energy levels omitted in the final model atom to the Pr III partition function is less than 0.01% at  $T_e = 7250$  K.

Levels of the same parity with small energy differences were combined into a single level. The final model atom includes 294 combined levels of Pr II, 54 combined levels of Pr III, and the ground state of Pr IV.

### 2.2. Radiative data

The 15788 and 392 radiative bound-bound transitions in Pr II and Pr III, respectively, are included in SE calculations. Oscillator strengths  $f_{ij}$  based on laboratory measurements of Lage & Whaling (1976) or estimated from the observed line intensities of Meggers et al. (1976) are available only for 448 transitions in Pr II. They come from the Kurucz & Bell (1995) linelist and are accessible via the Vienna Atomic Line Data Base (VALD, Kupka et al. 1999).

For the majority of transitions in Pr II and all transitions in Pr III, we rely, therefore, on oscillator strengths computed in

the present study. Calculations for Pr II are based on the wave functions obtained in the fittings of the energy levels. All the Hartree-Fock transition integrals are scaled by a factor 0.85. The calculated lifetimes have been compared with the recent accurate measurements of Scholl et al. (2002) and Biémont et al. (2003). A quite good agreement is found for the levels with leading contribution from the levels of the  $4f^3 6p$  configuration: the ratio of the measured to calculated lifetime equals 1.1 with a standard deviation 0.3. For the levels with highly mixed wave functions, the corresponding quantity appears to be 0.7 with the standard deviation 0.5. Details of these calculations can be found on [http://das101.isan.troitsk.ru/files/SPECTRA/Pr\\_II](http://das101.isan.troitsk.ru/files/SPECTRA/Pr_II) and will be presented in a forthcoming paper.

For Pr III, our approach follows that of Palmeri et al. (2000). Fitting of the energy levels is performed taking into account the interactions in the odd  $4f^3 + 4f^2 6p + 4f^5 d^2 + 4f^5 d 6s + 4f^6 s^2 + 4f^2 5f + 5p^5 4f^4$  and the even  $4f^2 5d + 4f^2 6d + 4f^2 6s + 5p^5 4f^3 5d + 5p^5 4f^3 6s + 4f^5 d 6p + 4f^6 s 6p + 4f^5 d 5f$  complexes. *Ab initio* transition integrals are taken. For 7 levels with a more than 25% contribution of the  $4f^2 6p$  configuration, the average ratio of the measured (Biémont et al. 2001) to calculated lifetimes is obtained to be  $1.17 \pm 0.25$ . An exception is the  $J = 9/2$  level at  $62535.6 \text{ cm}^{-1}$  with main contribution from the  $4f^5 d^2$  configuration and about 11% admixture of the  $4f^2 6p$  configuration. For this level, the lifetime ratio appears to be 3.1. Details of the Pr III calculations relevant to this article can be found on the website [http://das101.isan.troitsk.ru/files/SPECTRA/Pr\\_III](http://das101.isan.troitsk.ru/files/SPECTRA/Pr_III).

The photoionization cross-sections  $\sigma_{\text{ph}}$  are computed using the hydrogen approximation because no accurate data is available for the Pr II and Pr III levels. We assume that the photoionization from any Pr II level ends in the ground state of Pr III,  $4f^3 {}^4I_{9/2}$ . To take into account the photoionization to the remaining levels of the  $4f^3 {}^4I^\circ$  term we multiply  $\sigma_{\text{ph}}$  by the ratio  $g(4f^3 {}^4I^\circ)/g(4f^3 {}^4I_{9/2}) \simeq 5$ . The photoionization from the  $4f^2 5dnl$  levels ends in the excited Pr III  $4f^2 5d$  levels, however, we neglect this for the following reason. Replacing the real ending state on the Pr III ground state makes each  $4f^2 5dnl$  level to be easier ionized. Its ionization energy is reduced by more than 2 eV, and the photoionization rate is overestimated, in particular, for the levels with a threshold in the ultraviolet (UV). At the same time, the photoionization rates of the  $4f^2 5dnl$  levels are underestimated due to ignoring multiple channels for their ionization. We cannot estimate net effect due to absence of accurate atomic data.

### 2.3. Collisional data

The calculations of electron impact excitation and ionization rates rely on theoretical approximations. We use the formula of van Regemorter (1962) for the allowed transitions and assume that the effective collision strength  $\Upsilon = 1$  for the forbidden transitions. Electron impact ionization cross-sections are computed according to Drawin (1961).

The effects of the uncertainties of the used photoionization cross-sections and collisional rates on the final results are described in Sect. 6.3.

## 3. Programs and model atmospheres

The radiative transfer and the statistical equilibrium equations are solved with a revised version of the DETAIL program (Butler & Giddings 1985) using the accelerated lambda iteration fol-

lowing the extremely efficient method described by Rybicki & Hummer (1991, 1992). Background opacities include the important bound-free and free-free transitions of hydrogen, helium, and the most abundant metals, the Rayleigh scattering, the Thomson scattering, the hydrogen lines, the quasi-molecular Lyman  $\alpha$  satellites due to H-H and H-H<sup>+</sup> collisions (Allard et al. 1998), and line opacity calculated with the line lists made available by Kurucz & Bell (1995). The background opacities are sampled on a random grid of 4500 frequencies, to which are added the frequencies of the line profiles. The final non-LTE line formation program samples roughly 150 000 wavelengths between 500 Å and 80 000 Å.

The obtained non-LTE and LTE level populations are used to compute the emergent flux, line profiles, and equivalent widths with the code LINEC. The investigated lines and transitions of Pr II and Pr III are listed in Table 2. The wavelengths of Pr II lines are taken from Ginibre (1990). Ritz wavelengths are used for the Pr III lines.

Hyperfine-structure (HFS) affecting the Pr II lines is explicitly calculated with the HFS constants given by Ginibre (1989a), if available. No HFS data exist in the literature for the Pr III lines. Ivarsson et al. (2001, ILW) could not resolve HFS in any of the accurately measured Pr III lines, which means that HFS is not large, although some lines show asymmetric profiles with half-widths exceeded the half-width of the resolved HFS components in Pr II. The three from eight common Pr III lines are practically HFS unaffected according to the ILW laboratory analysis. Half-widths of other three lines are three to four times larger compared to those for the HFS unaffected lines, and they are comparable with the thermal half-widths of the Pr III lines in the atmosphere of HD 24712. The thermal half-width of the Pr lines corresponds to approximately  $1 \text{ km s}^{-1}$ . Our simulation of HFS affecting the Pr III 5998 and 6053 lines with the strongest HFS broadening according to the measurements of Ivarsson et al. (2001) leads to an increase of the theoretical equivalent widths, by 16 mÅ and 17 mÅ, respectively, that transforms to  $-0.20$  dex and  $-0.24$  dex decrease of the element abundance derived from these lines. Further analysis is performed not accounting for HFS for the Pr III lines. We show in Sect. 6.2, that two abovementioned lines give the results consistent with those for the Pr III lines with weak HFS broadening.

We use homogeneous blanketed model atmospheres. The small grid of models with  $T_{\text{eff}}$  ranging between 7500 K and 9500 K with a step of 500 K,  $\log g = 4$ , and the solar chemical composition has been calculated with the MAFAGS code (Fuhrmann et al. 1997) that treats line-blanketing using the opacity distribution functions (ODF). The original ODF tables of Kurucz (1994a) were scaled by  $-0.16$  dex to put the iron opacity calculated by Kurucz with  $\log \varepsilon_{\text{Fe}} = 7.67$  into correspondence with a value  $\log \varepsilon_{\text{Fe}} = 7.51$  which we believe to be the best representation of the solar mixture. We refer to abundances on the usual scale where  $\log \varepsilon_{\text{H}} = 12$ .

For HD 24712 ( $T_{\text{eff}} = 7250 \text{ K}$ ,  $\log g = 4.3$ ,  $[M/H] = 0$  according to Ryabchikova et al. 1997), the model atmosphere has been computed by Frank Grupp with the MAFAGS-OS code (Grupp 2004). It is based on up-to-date continuous opacities and includes the effects of line-blanketing through opacity sampling.

HD 24712 possesses a magnetic field with a mean magnetic field modulus  $\langle B \rangle$  changing from 2.5 kG at the magnetic minimum to  $\sim 3.1$ – $3.3$  kG at the magnetic maximum (Ryabchikova et al. 2007b). We ignore the influence of the magnetic field on atmospheric structure, based on the results of Kochukhov et al. (2005) who have shown that the difference in temperature and

gas pressure distributions between magnetic and non-magnetic model atmospheres with  $T_{\text{eff}} = 8000$  K does not exceed 30 K and 6%, respectively, for field strengths up to 5 kG. However, splitting of the spectral lines in the magnetic field is taken into account in LTE abundance analysis. Magnetic spectrum synthesis is performed with the help of SYNTHMAG code (Kochukhov 2007).

There are observational evidences for non-uniform element distribution in the atmosphere of HD 24712. The neodymium is strongly enhanced in the uppermost atmospheric layers according to Mashonkina et al. (2005). Ryabchikova et al. (2008) and Ryabchikova (2008) show that Ca, Si, Cr, Fe, Sr, and Ba are concentrated in deep atmospheric layers. One believes that radiatively driven diffusion is one of the main processes responsible for these inhomogeneities. The self-consistent diffusion models predict the vertical distributions of Mg, Si, Ca, Ti, Fe which qualitatively reproduce the corresponding element stratifications found empirically for some Ap stars (Alecian & Stift 2007, LeBlanc & Monin 2004). But no theoretical predictions are available for the REE due to an incompleteness of atomic data on energy levels and transition probabilities. Stratified distribution of chemical elements in the atmosphere can influence the atmospheric structure. Modelling chemically non-uniform stellar atmospheres based on the abundance gradients determined empirically is in progress (Shulyak, 2008, private communication). Preliminary results of the iterative procedure for HD 24714 predict the slight change in the model parameters ( $T_{\text{eff}} = 7250$  K and  $\log g = 4.1$ ) and lead to only minor changes in our results on Pr analysis presented in Sect. 6.

#### 4. Departures from LTE for Pr II-Pr III

In line formation layers of the atmospheres with  $T_{\text{eff}}$  between 7250 K and 8000 K, number density of Pr II is larger compared to that for Pr III (see Fig. 4). However, Pr II drops rapidly in the hotter atmospheres. Non-LTE calculations show that the main non-LTE effect for Pr II is overionization caused by a super-thermal radiation of non-local origin near the thresholds of the  $4f^36p$  levels with  $E_{\text{exc}} = 3$  eV – 4 eV ( $\lambda_{\text{thr}} = 1600\text{\AA}$  to  $1850\text{\AA}$ ). Photoionization is able to drain the populations of these levels in the model with the lowest temperature,  $T_{\text{eff}} = 7250$  K, and the effect is strengthened with  $T_{\text{eff}}$  increasing. The population loss is redistributed over many levels, producing overall depletion of the first ionization stage in line formation layers. In contrast, photoionization of the Pr III levels is inefficient due to very low stellar fluxes in the far ultraviolet ( $\lambda < 900\text{\AA}$ ), where the ionization edges of the Pr III ground state and the low excitation levels are located. At  $T_{\text{eff}} \leq 8000$  K, overionization of Pr II leads to overpopulation of Pr III. At the higher temperatures, Pr III represents the majority of the element and preserves the thermodynamic equilibrium (TE) total number density.

We find that the mechanisms driving departures from LTE for Pr II/III are similar in the atmospheres with uniform and stratified distribution of praseodymium, however, the magnitude of the effect is different due to a different location of the line formation layers.

##### 4.1. The atmospheres with uniform distribution of praseodymium

In the observed spectrum of HD 24712, 14 lines of Pr III are detected with a measured equivalent width,  $W_\lambda$ , of 17 mÅ and larger. In order to predict the equivalent widths of the Pr III

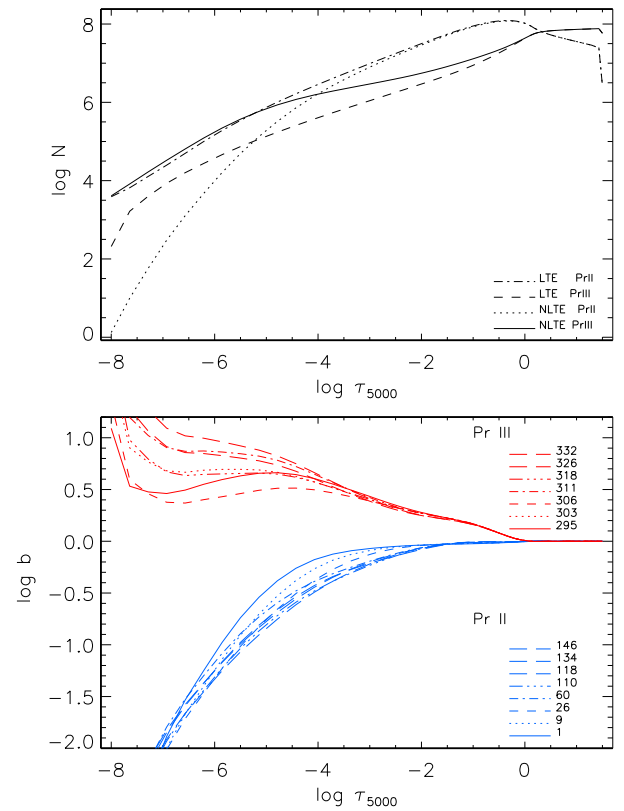


**Fig. 4.** LTE and non-LTE total number densities of Pr II and Pr III (top panel) and departure coefficients for selected levels of Pr II and Pr III (bottom panel) in the model atmosphere 7250/4.3/0. Successive numbers of the levels in our model atom are quoted. Everywhere in the atmosphere  $[\text{Pr}/\text{H}] = 3$ .

lines at a detectable level in the model, which represents the atmosphere of HD 24712, we perform calculations with the praseodymium abundance  $[\text{Pr}/\text{H}] = 3$ . This value also characterizes the mean Pr abundance derived from all investigated Pr II and Pr III lines in HD 24712. Figure 4 shows the departure coefficients,  $b_i = n_i^{\text{NLTE}}/n_i^{\text{LTE}}$  of the selected levels of Pr II and Pr III as a function of continuum optical depth  $\tau_{5000}$  at  $\lambda = 5000\text{\AA}$  in the model atmosphere with  $T_{\text{eff}}/\log g/[\text{M}/\text{H}] = 7250/4.3/0$ . Here,  $n_i^{\text{NLTE}}$  and  $n_i^{\text{LTE}}$  are the statistical equilibrium and TE (Saha-Boltzmann) number densities, respectively. The medium becomes optically thin for the ionizing radiation below  $1850\text{\AA}$  far inside the atmosphere, at  $\log \tau_{5000}$  around 0. As a result, Pr III is overpopulated in line formation layers, at  $\log \tau_{5000} < 0$ . The Pr II levels with  $E_{\text{exc}} < 6$  eV are strongly coupled to the Pr II ground state and to each other inside  $\log \tau_{5000} \approx -1.7$  where their departure coefficients are only slightly below 1. The outside layers become transparent for the radiation of many Pr II lines arising between low-excitation terms ( $E_{\text{exc}} < 2$  eV) and intermediate-excitation terms ( $E_{\text{exc}} = 2.7 - 4$  eV). The photon loss in these lines amplifies the underpopulation of the upper levels (level numbers from 110 to 146 in Fig. 4) caused by enhanced photoionization.

The non-LTE effect on the line strength is determined by the departures from LTE for the lower and upper levels of the transition in the line formation layers. For the model 7250/4.3/0, the non-LTE effects are very small for the Pr II lines. The obtained

**Table 2.** Investigated transitions in Pr II and Pr III.

| $\lambda$ [Å]         | $E_{\text{exc}}$ (eV) | Transition                                      |                      |
|-----------------------|-----------------------|---|----------------------|
| Pr II                 |                       |   |                      |
| 4222.93 <sup>1*</sup> | 0.05                  | $4f^3 5d^5 I_5^\circ - 4f^3 6p^5 K_6$           | 2 - 118 <sup>2</sup> |
| 4449.83 <sup>1*</sup> | 0.20                  | $4f^3 5d^5 I_6^\circ - 4f^3 6p^5 K_6$           | 3 - 118              |
| 5002.44               | 0.80                  | $4f^3 5d^5 K_7^\circ - 4f^3 6p^3 K_6$           | 12 - 129             |
| 5110.76 <sup>*</sup>  | 1.15                  | $4f^3 5d^5 I_{10}^\circ - 4f^3 6p^5 K_9$        | 26 - 143             |
| 5129.54 <sup>*</sup>  | 0.65                  | $4f^3 5d^5 K_6^\circ - 4f^3 6p^5 I_5$           | 10 - 121             |
| 5135.14 <sup>*</sup>  | 0.95                  | $4f^3 5d^5 K_8^\circ - 4f^3 6p^5 K_8$           | 16 - 134             |
| 5259.73 <sup>1*</sup> | 0.63                  | $4f^3 5d^5 L_7^\circ - 4f^3 6p^5 K_6$           | 9 - 118              |
| 5292.62 <sup>*</sup>  | 0.65                  | $4f^3 5d^5 K_6^\circ - 4f^3 6p^5 K_6$           | 10 - 118             |
| 5322.77 <sup>*</sup>  | 0.48                  | $4f^3 5d^5 L_6^\circ - 4f^3 6p^5 K_5$           | 6 - 110              |
| 5681.88               | 1.16                  | $4f^3 5d^5 H_3^\circ - 4f^2 5d^2 \text{}^3 G_5$ | 26 - 134             |
| 6017.80 <sup>*</sup>  | 1.11                  | $4f^3 5d^5 G_2^\circ - 4f^3 6p^5 H_3$           | 23 - 126             |
| 6165.94 <sup>*</sup>  | 0.92                  | $4f^3 5d^5 I_4^\circ - 4f^3 6p^5 I_4$           | 15 - 116             |
| 6656.83 <sup>*</sup>  | 1.82                  | $4f^3 5d^3 L_9^\circ - 4f^3 6p^3 K_8$           | 60 - 146             |
| Pr III                |                       |   |                      |
| 4910.82               | 0.17                  | $4f^3 4I_{11/2}^\circ - 4f^2 5d^4 H_{11/2}$     | 296 - 322            |
| 4929.12               | 0.36                  | $4f^3 4I_{13/2}^\circ - 4f^2 5d^4 H_{13/2}$     | 297 - 325            |
| 5284.69               | 0.17                  | $4f^3 4I_{11/2}^\circ - 4f^2 5d^4 H_{9/2}$      | 296 - 319            |
| 5299.99               | 0.36                  | $4f^3 4I_{13/2}^\circ - 4f^2 5d^4 H_{11/2}$     | 297 - 322            |
| 5844.41               | 1.24                  | $4f^3 2H_{9/2}^\circ - 4f^2 5d^2 G_{7/2}$       | 300 - 332            |
| 5998.97               | 0.17                  | $4f^3 4I_{11/2}^\circ - 4f^2 5d^4 G_{9/2}$      | 296 - 315            |
| 6053.00               | 0.00                  | $4f^3 4I_{9/2}^\circ - 4f^2 5d^4 G_{7/2}$       | 295 - 311            |
| 6090.01               | 0.36                  | $4f^3 4I_{13/2}^\circ - 4f^2 5d^4 H_{11/2}$     | 297 - 318            |
| 6160.23               | 0.17                  | $4f^3 4I_{11/2}^\circ - 4f^2 5d^4 H_{9/2}$      | 296 - 314            |
| 6195.62               | 0.00                  | $4f^3 4I_{9/2}^\circ - 4f^2 5d^4 H_{7/2}$       | 295 - 310            |
| 6500.04               | 1.72                  | $4f^3 2G_{7/2}^\circ - 4f^2 5d^2 F_{5/2}$       | 306 - 334            |
| 6616.46               | 1.55                  | $4f^3 2H_{11/2}^\circ - 4f^2 5d^4 F_{9/2}$      | 303 - 332            |
| 6692.25               | 1.16                  | $4f^3 4F_{3/2}^\circ - 4f^2 5d^4 F_{3/2}$       | 299 - 326            |
| 6706.70               | 0.55                  | $4f^3 4I_{15/2}^\circ - 4f^2 5d^2 I_{13/2}$     | 298 - 318            |

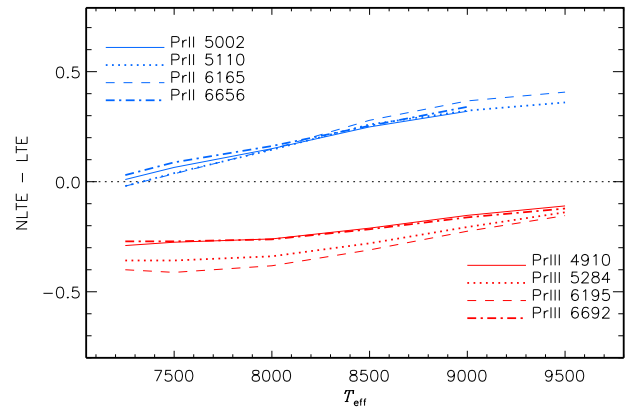
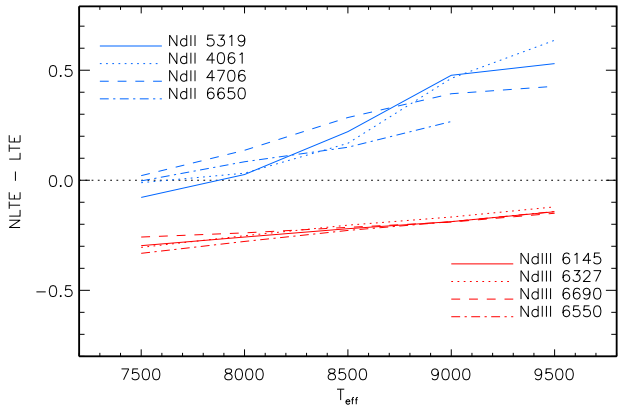
<sup>1</sup> Lines used only for solar abundance analysis.<sup>2</sup> The level numbers in the model atom.

\* HFS is taken into account.

overpopulation of the Pr III levels leads to the strengthening of the Pr III lines compared with the LTE case. The theoretical non-LTE and LTE equivalent widths of the selected lines and the non-LTE abundance corrections  $\Delta_{\text{NLTE}} = \log \epsilon_{\text{NLTE}} - \log \epsilon_{\text{LTE}}$  are presented in Table 4 (columns 6 – 8). Oscillator strengths used in these calculations are taken from Kurucz & Bell (1995) for the Pr II lines and are computed in this paper for the lines of Pr III.

As expected, the departures from LTE for the Pr II lines grow with  $T_{\text{eff}}$ . The larger  $T_{\text{eff}}$ , the stronger ultraviolet radiation is, thus resulting in amplified overionization of Pr II. Figure 5 shows the calculated non-LTE abundance corrections for some lines of Pr II and Pr III depending on  $T_{\text{eff}}$ . Everywhere,  $[\text{Pr}/\text{H}] = 3$  is adopted. For the Pr II lines,  $\Delta_{\text{NLTE}}$  are positive. They are small at  $T_{\text{eff}} = 7250$  K and 7500 K with  $\Delta_{\text{NLTE}} < 0.1$  dex and grow to approximately 0.4 dex at  $T_{\text{eff}} = 9500$  K. In the hottest model, Pr II  $\lambda 5002$  and  $\lambda 6656$  have  $W_\lambda \leq 1$  mÅ, and their  $\Delta_{\text{NLTE}}$  are not shown. In contrast, the departures from LTE for Pr III are weakened toward higher  $T_{\text{eff}}$  because doubly-ionized praseodymium tends to represent the majority of the element and to preserve the TE total number density. The non-LTE abundance corrections are negative for the Pr III lines with  $\Delta_{\text{NLTE}} \approx (-0.3) - (-0.4)$  dex at  $T_{\text{eff}} = 7500$  K and  $\Delta_{\text{NLTE}} \approx -0.1$  dex at  $T_{\text{eff}} = 9500$  K.

In this paper, we present also the revised non-LTE abundance corrections for the Nd II and Nd III lines (Fig. 6). Opacity package of the DETAIL code was recently updated by the inclusion of the quasi-molecular Lyman  $\alpha$  satellites following Castelli & Kurucz (2001) implementation of the Allard et al. (1998) theory and by

**Fig. 5.** Non-LTE abundance corrections for the Pr II and Pr III lines depending on  $T_{\text{eff}}$ . For all models,  $\log g = 4$ . The calculations were made with the Pr abundance  $[\text{Pr}/\text{H}] = 3$ .**Fig. 6.** Non-LTE abundance corrections for the Nd II and Nd III lines depending on  $T_{\text{eff}}$ . For all models,  $\log g = 4$ . The calculations were made with the Nd abundance  $[\text{Nd}/\text{H}] = 2.5$ .

the use of the extended line list based on not only measured but also predicted lines from Kurucz & Bell (1995). The effect of the increased UV opacity below  $1700\text{\AA}$  is seen only for the lines of Nd II at  $T_{\text{eff}} \geq 8500$  K. At the lower temperatures, the revised  $\Delta_{\text{NLTE}}$  of the Nd II lines agree within 0.01 dex to 0.03 dex with that obtained by Mashonkina et al. (2005). For the Nd III lines, the maximal difference between the revised and 2005's  $\Delta_{\text{NLTE}}$  constitutes 0.05 dex at  $T_{\text{eff}} = 8500$  K and is smaller at the lower and higher temperatures. Thus, the Nd abundance distributions in the atmospheres of HD 24712 ( $T_{\text{eff}} = 7250$  K) and  $\gamma$  Equ ( $T_{\text{eff}} = 7700$  K) found in our earlier paper do not need to be revised. For the Nd II lines at  $T_{\text{eff}} \geq 8500$  K, we obtain now the smaller departures from LTE due to decreased ionizing radiation. The difference in  $\Delta_{\text{NLTE}}$  equals 0.1 dex to 0.2 dex for different lines at different temperatures.

#### 4.2. The atmospheres with stratified distribution of praseodymium

In this section, the departures from LTE for Pr II/III are investigated in the model 7250/4.3/0 with the stratified Pr abundance distribution determined in Sect. 6.2 and shown by continuous



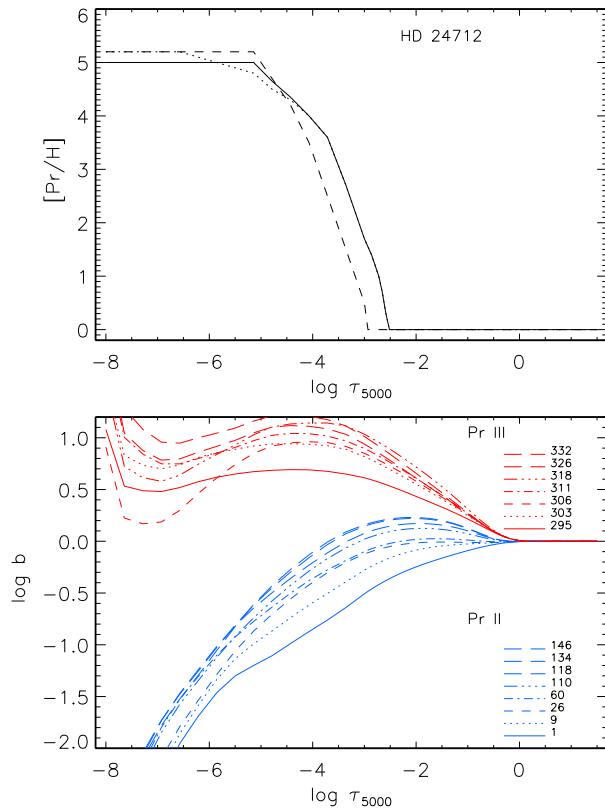


**Fig. 7.** Top panel: the  $[\text{Pr}/\text{H}]$  ratio distributions found in the atmosphere of HD 24712 (continuous line) and from the test calculations with 2 dex smaller photoionization cross-sections (dashed line) and with a variable effective collision strength for forbidden transitions (dotted line). Bottom panel: the departure coefficients  $\log b$  for the selected levels of Pr II and Pr III in the model 7250/4.3/0 representing the atmosphere of HD 24712 from calculations with the praseodymium distribution shown in the top panel by continuous curve. See text for more details.

curve in the top panel of Fig. 7. The departure coefficients for the selected levels of Pr II and Pr III are shown in the bottom panel of the same figure. The theoretical non-LTE and LTE equivalent widths together with non-LTE abundance corrections are given in Table 4 (columns 9 – 11).

Non-LTE calculations show the depletion of Pr II and enhanced number density of Pr III in the line formation layers similar to the case of homogeneous Pr abundance distribution. However, three important distinctions in the behavior of departure coefficients can be seen.

- The magnitude of the depletion of Pr II is much larger in the stratified atmosphere, in particular, above  $\log \tau_{5000} = -4$  where the lines are formed.
- In the stratified atmosphere, for every pair of the Pr II levels with  $i < j$ , an inequality  $b_i < b_j$  is valid.
- Above  $\log \tau_{5000} = -4$  in the stratified atmosphere, the excited levels of Pr III are decoupled to the ground state to the more extent compared to the case of the homogeneous Pr abundance distribution.

In the stratified atmosphere, the Pr lines are formed in the uppermost atmospheric layers, above  $\log \tau_{5000} = -4$ , where the

departures from LTE are large. Non-LTE leads to weakening the Pr II lines due to the decreased number of absorbers ( $b_i < 1$ ) and due to the line source function  $S_{ij} \approx b_j/b_i B_\nu(T_e)$  exceeding the Planck function ( $b_i < b_j$ ). The non-LTE abundance corrections for various Pr II lines are positive and may reach +1.2 dex. The Pr III lines are strengthened compared with the LTE case, and  $\Delta_{\text{NLTE}}$  may reach  $-0.7$  dex. Since the non-LTE effects have the opposite sign for the Pr II and Pr III lines, they are important for the comparison of Pr abundances derived from these lines.

## 5. Solar abundance of praseodymium

We first apply the non-LTE calculations to the Pr abundance analysis for the solar atmosphere. The earlier determinations were performed by Biémont et al. (1979) based on the nine lines of Pr II in the 3990 – 5330 Å spectral region and by Ivarsson et al. (2003) based on the three lines of Pr II. The obtained mean abundances of the praseodymium are surprisingly different,  $\log (\text{Pr}/\text{H})_\odot = -11.29 \pm 0.08$  and  $\log (\text{Pr}/\text{H})_\odot = -11.60 \pm 0.1$ , respectively. The most recent study is based on the modern accurate laboratory measurements for oscillator strengths of Ivarsson et al. (2001). Ivarsson et al. (2003) also test the influence of 3D effects on the determination of the Pr abundance and draw a preliminary conclusion that the differences in the equivalent widths of the Pr II lines between the 3D and 1D cases are insignificant.

Each of the lines used by our predecessors was checked for blending using the NSO solar flux spectrum (Kurucz et al. 1984) observed with the spectral resolving power  $R \approx 340000$  at wavelengths between 4000 Å and 4700 Å and with  $R = 520000$  at longer wavelengths. We find four lines suitable for precise spectral fitting. They are listed in Table 3. Spectral region around each investigated line was synthesised with the SIU code (Reetz 1991). For given atomic level, SIU computes the non-LTE population as the production of the LTE occupation number and the corresponding departure coefficient. In LTE calculations, the revised Pr II partition function is applied. Calculations of the Pr II lines were made with the three different sets of transition probabilities taken from Kurucz & Bell (1995), Ivarsson et al. (2001), and Li et al. (2007). Atomic parameters for other atomic lines in the synthesised regions are taken from the latest release of VALD (Kupka et al. 1999). For molecular lines, we apply the data compiled by Kurucz (1994b). We use the theoretical ATLAS9 model atmosphere of the Sun (5777/4.44/0, Heiter et al. 2002) with convection treated according to Canuto et al. (1996) and the semi-empirical model of Holweger & Müller (1974, HM). A microturbulence velocity  $V_{\text{mic}} = 0.9 \text{ km s}^{-1}$  is adopted. Our synthetic flux profiles are convolved with a profile that combines a rotational broadening of  $1.8 \text{ km s}^{-1}$ , broadening by macroturbulence with a radial-tangential profile of  $V_{\text{mac}} = 3.6 \text{ km s}^{-1}$ , and instrumental broadening with a Gaussian profile corresponding to the spectral resolution. A macroturbulence velocity was allowed to vary within  $0.2 \text{ km s}^{-1}$  to achieve the best fit to the observed line shape.

The best fits to the observed solar line profiles are shown in Fig. 8. The results from calculations with the ATLAS9 solar model atmosphere are presented in Table 3. Below we give brief notes on the individual lines.

**Pr II 4222.93 Å.** The continuum flux at 4222.93 Å is influenced by the far wing of the Ca I resonance line at 4226.7 Å. The Ca I line is treated using the measured oscillator strength from Smith & Gallagher (1966) and the van der Waals broadening parameters based on the advanced perturbation theory of Anstee & O'Mara (1995). The Pr II 4222.93 Å line is partially

overlapped with the blue wing of the spectral feature produced by two CH lines at 4223.091 Å and 4223.113 Å. A half-width of this spectral feature is only slightly affected by the Pr II line and is fitted reasonably well if we reduce oscillator strengths for both CH lines by 0.3 dex compared to those given by Kurucz (1994b). Small changes in wavelengths (no more than 0.014 Å) and oscillator strengths (no more than 0.27 dex) were introduced to fit the Cr I 4222.740 Å and Fe I 4223.237 Å lines just to make better fit.

**Pr II 5259.7 Å.** This line is well isolated and very well fitted by spectrum synthesis. The Ni I 5259.466 Å and Ti I 5259.973 Å lines shown in Fig. 8 do not affect the Pr abundance determination. For the Ni I line, changes in wavelength by 0.011 Å and in oscillator strength by  $-0.4$  dex were made to fit the line profile, while a 0.005 Å wavelength change is required for Ti I line.

**Pr II 5322.8 Å** is well isolated, too, but the continuum flux is influenced by the far wing of the Fe I 5324.179 Å line. With the best atomic parameters of the Fe I line,  $\log gf = -0.103$  (Bard et al. 1991) and  $\log \gamma_6/N_H = -7.035$  at  $T_e = 10000$  K (increased by 0.2 dex compared with the Anstee & O'Mara's 1995 value), the predicted synthetic spectrum is still 0.2% higher than the observed spectrum around 5323 Å. The local continuum level was, therefore, adjusted to fit the blue wing of Fe I 5324 Å. A variation of 0.2% in the continuum flux produces a 0.05 dex change in the Pr abundance derived from Pr II 5322.8 Å.

**Pr II 4449.83 Å** is located between the Dy II 4449.70 Å and Si I 4449.90 Å lines. The blue wing and the core of the Dy II line are slightly affected by the adjacent lines and are well fitted using a center line wavelength of 4449.707 Å, accurate experimental oscillator strength,  $\log gf = -1.03$  (Wickliffe et al. 2000), and the solar Dy abundance  $\log \epsilon_{Dy,\odot} = 1.14$  (Lodders 2003). The Si I line is predicted, and its oscillator strength has to be reduced down to  $\log gf = -3.33$  to fit the line core that is only slightly affected by the HFS components of the Pr II line. In Fig. 8, we show the best fit of the 4449 Å blend and also the synthetic spectra computed with  $\pm 0.05$  dex change in adopted Pr abundance. The uncertainty of the element abundance derived from Pr II 4449 is, obviously, does not exceed 0.05 dex.

In the solar atmosphere, Pr II represents the majority of the element, and its ground state and the low excitation levels which are the lower levels of the investigated transitions preserve the TE number density. Our non-LTE calculations show that photon pumping produces enhanced excitation of the upper levels resulting in weakening the lines of interest compared to the LTE case. We find that the statistical equilibrium of Pr II in the solar atmosphere is sensitive to a variation of collision excitation rates which include, for the Sun, interactions with not only electrons but also neutral hydrogen atoms. For hydrogenic collisions, we use the formula of Steenbock & Holweger (1984) for allowed transitions and follow Takeda (1994) for forbidden transitions. Both theoretical approximations provide only an order of magnitude estimate. Empirical constraining the efficiency of hydrogenic collisions in the SE of various atoms that is represented by a scaling factor  $S_H$  applied to the mentioned formula gives a variety of estimates between  $S_H = 0.002$  and  $S_H = 1$  (for review, see Mashonkina 2008). When pure electronic collisions are taken into account ( $S_H = 0$ ), the non-LTE abundance corrections constitute +0.03 dex to +0.08 dex for different lines. The non-LTE effects become negligible ( $\Delta_{NLTE} \leq 0.01$  dex) when both types of collisions are included and  $S_H = 1$ . We adopt an intermediate value,  $S_H = 0.1$ . The corresponding non-LTE corrections are shown in the last column of Table 3.

The average LTE and non-LTE praseodymium abundances from calculations with the ATLAS9 solar model atmosphere and their standard deviations are presented in two bottom strings of Table 3. The Pr abundance determined with the HM model is larger, by 0.05 dex, on average. It is worth noting that the statistical error of our abundance determination estimated from the line-to-line scatter corresponds, in fact, to the quoted errors of  $\log gf$  measurements which varies between 0.03 dex and 0.07 dex for the lines in Table 3. The three solutions found with  $\log gf$  from different sources are consistent within the error bars. However, the preference should be given to the ILW and LCH abundances based on the modern experimental transition probabilities. The average ILW and LCH abundances agree within 0.01 dex. For each set of atomic parameters and for both solar model atmospheres, the derived Pr abundance is 0.09 dex  $-$  0.23 dex larger than that obtained by Biémont et al. (1979) and 0.40 dex  $-$  0.54 dex larger compared to that of Ivarsson et al. (2003). Different studies give the meteoritic CI Chondrites abundance  $\log (Pr/H)_{\text{met}} = -11.20 \pm 0.04$  (Grevesse et al. 1996; Palme & Jones 2005),  $-11.22 \pm 0.03$  (Lodders 2003) or  $-11.25 \pm 0.03$  (Asplund et al. 2005). Our best solar Pr abundance for the ATLAS9/HM model,  $\log (Pr/H)_{\odot} = -11.15 \pm 0.08$  /  $-11.10 \pm 0.08$ , exceeds the meteoritic values by 0.05 dex to 0.10 dex.

In solar abundance determinations, we use the partition function calculated by its definition and based on an extensive set of the predicted energy levels of Pr II,  $U_{\text{calc}}(Pr II)$ . As can be seen from Table 1,  $U_{\text{calc}}(Pr II)$  is about 30% larger than that for the experimental energy levels only,  $U_{\text{exp}}(Pr II)$ , at temperatures of the line formation layers in the solar atmosphere.

With  $U_{\text{exp}}(Pr II)$ , the inferred solar Pr abundance is  $\log (Pr/H)_{\odot} = -11.22$  and  $-11.17$ , for the ATLAS9 and the Holweger & Müller (1974) models, respectively. Thus, accurate solar Pr abundance depends on the completeness of known Pr II levels and on the accuracy of their energies. It seems that the current theoretical energy calculations give us the upper limit for the solar Pr abundance.

## 6. Praseodymium in the roAp star HD 24712

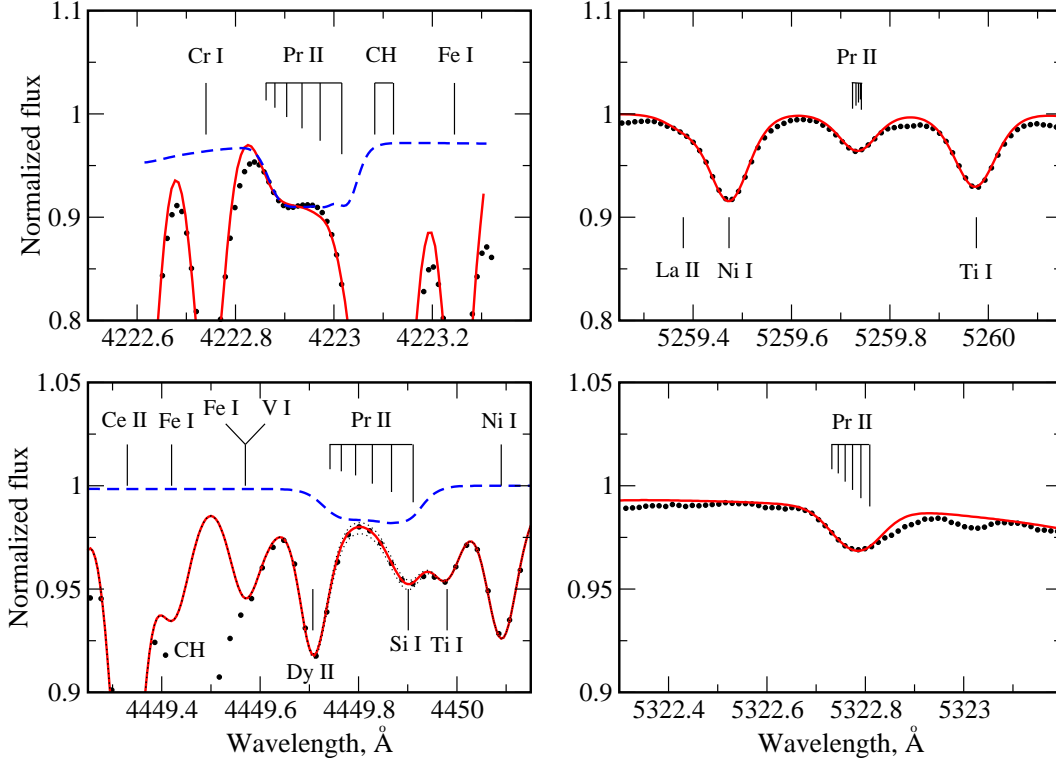
We study the Pr abundance in the atmosphere of the roAp star HD 24712 using its average spectrum obtained during spectroscopic monitoring on November 11/12, 2004 with the UVES spectrograph at the 8.2-m telescope, UT2 (Kueyen), of the VLT on Paranal, Chile (programme 274.D-5011). Observations and data reduction are described by Ryabchikova et al. (2007b). The spectrum has been obtained near the magnetic maximum, that coincides roughly with the REE spectral line intensity maximum. The surface magnetic field measured at the magnetic maximum is  $\langle B \rangle = 3.1 - 3.3$  kG (Ryabchikova et al. 2007b).

### 6.1. The problem of the Pr abundance in HD 24712

We start from element abundance determination using the lines of Pr II and Pr III listed in Table 4 and assuming the uniform distribution of Pr in the atmosphere of HD 24712. The choice of the spectral lines was determined mainly by the possibility of pulsation measurements in the HD 24712 spectrum. Magnetic spectrum synthesis is performed with the help of SYNTHMAG code under the LTE assumption using the model atmosphere 7250/4.3/0. We apply most recent experimental transition probabilities by Ivarsson et al. (2001) and Li et al. (2007) if available and oscillator strengths from Kurucz & Bell (1995) for the remaining Pr II lines. The derived LTE abundance is  $\log (Pr/H) =$

**Table 3.** Solar praseodymium abundance from calculations with the ATLAS9 solar model atmosphere.

| $\lambda$ [Å] | log $gf$        |                  |                  | log (Pr/H) <sub>LTE</sub> |                   |                   | $\Delta_{\text{NLTE}}$ |
|---------------|-----------------|------------------|------------------|---------------------------|-------------------|-------------------|------------------------|
|               | KB <sup>1</sup> | ILW <sup>2</sup> | LCH <sup>3</sup> | KB                        | ILW               | LCH               |                        |
| 4222.93       | 0.13            | 0.27             | 0.24             | -11.14                    | -11.28            | -11.25            | +0.03                  |
| 4449.83       | -0.32           | -0.17            | -0.26            | -11.07                    | -11.22            | -11.13            | +0.02                  |
| 5259.73       | 0.08            | 0.11             | 0.07             | -11.11                    | -11.14            | -11.10            | +0.04                  |
| 5322.77       | -0.32           | -0.32            | -0.12            | -11.04                    | -11.04            | -11.24            | +0.02                  |
|               | LTE-average     |                  |                  | -11.09 $\pm$ 0.04         | -11.17 $\pm$ 0.10 | -11.18 $\pm$ 0.08 |                        |
|               | non-LTE-average |                  |                  | -11.06 $\pm$ 0.04         | -11.14 $\pm$ 0.10 | -11.15 $\pm$ 0.08 |                        |

<sup>1</sup> Kurucz & Bell (1995, KB)<sup>2</sup> Ivarsson et al. (2001, ILW)<sup>3</sup> Li et al. (2007, LCH)**Fig. 8.** Synthetic spectra (continuous curve) and pure Pr II line profiles (dashed curve, for  $\lambda 4223$  Å and  $\lambda 4449$  Å lines only) calculated with the ATLAS9 solar model atmosphere in comparison with the observed NSO solar flux spectrum (Kurucz et al. 1984, bold dots). For the 4449 Å blend, dotted lines show the synthetic spectra computed with  $\pm 0.05$  dex change in the adopted Pr abundance. The Pr II lines are treated based on non-LTE line formation.

$-9.4 \pm 0.2$  from 10 Pr II lines and by 2.1 dex larger,  $\log(\text{Pr}/\text{H}) = -7.3 \pm 0.3$ , from 14 Pr III lines. Such a large discrepancy between the rare-earth LTE abundances derived from two ionization stages is typically observed in the roAp and cool Ap stars (the REE anomaly, see Ryabchikova et al. 2004).

Our non-LTE code does not include the magnetic field in statistical equilibrium calculations. The presence of a magnetic field should not cause significant changes in the derived level populations, for moderate field strengths. As was shown in Sect. 4, departures from LTE for the level populations are mainly caused by UV continua and by strong UV transitions. The change in emergent continuum flux around 2000 Å due to the influence of the magnetic field on atmospheric structure does not exceed 7%, for field strengths up to 10 kG (Kochukhov et al. 2005). The critical strong UV transitions have small Zeeman splittings, since the splittings scale with the wavelength. Further abundance determinations are, therefore, performed in the field-free approximation.

With fixed level populations, the magnetic field can affect an abundance analysis through Zeeman splitting of spectral lines. Therefore, we investigate a possibility to replace magnetic broadening effects by other broadening mechanisms, for instance, by a microturbulence. Different spectral lines used in this study have different Zeeman patterns. The Pr II lines are weak and HFS-affected. We adopt a common value,  $V_{\text{mic}} = 1 \text{ km s}^{-1}$ , in their analysis. For each line of Pr III, a pseudo-microturbulence velocity is calculated as follows. We first fit the line profile with the SYNTHMAG code to derive the Pr abundance in LTE approximation. Then, calculations are made with the SYNTH3 code (Kochukhov 2007) that ignores the existence of magnetic field. The element abundance is fixed and  $V_{\text{mic}}$  varies until the theoretical equivalent width reaches the observed one. The individual values of  $V_{\text{mic}}$  are given in Table 4. Applying this procedure we find only minor changes in the element abundances, by 0.14 dex and 0.16 dex from the Pr II and Pr III lines, respectively, compared to those determined from magnetic spectrum synthe-



sis. It is worth noting, that the abundance difference between two ionization stages remains to be almost the same.

Next, we check whether the departures from LTE can solve the problem of the praseodymium abundance in HD 24712 and find that non-LTE tends to reduce the difference in LTE abundances but fails to remove it completely. The non-LTE abundance is  $\log(\text{Pr}/\text{H}) = -9.22 \pm 0.19$  from the  $\text{Pr II}$  lines, and a 1.90 dex larger value is determined from the lines of  $\text{Pr III}$ . Thus, we cannot obtain consistent abundances of the praseodymium from the lines of two ionization stages assuming the uniform element distribution in the atmosphere of HD 24712, either considering non-LTE line formation, or taking into account the splitting of the spectral lines in magnetic field. We suggest, therefore, that similarly to the neodymium (Mashonkina et al. 2005) the praseodymium is distributed non-uniformly in the atmosphere of HD 24712, although the properties of the Nd and Pr distributions may be different.

### 6.2. Vertical distribution of Pr in the atmosphere

Using the simplified step-function approximation as an initial guess for the Pr abundance profile, we modify it by the trial-and-error method based on non-LTE line formation trying to fit the observed equivalent widths of both  $\text{Pr II}$  and  $\text{Pr III}$  lines in the spectrum of HD 24712. Due to certain limitations of the present non-LTE calculations, mainly due to ignoring Zeeman splitting, we cannot use the observed line profiles in stratification analysis as this was done, for instance, in LTE analysis for Ca (Ryabchikova et al. 2008). The final solution is shown in the top panel of Fig. 7. The praseodymium is concentrated mostly above  $\log \tau_{5000} = -4$ , and the required Pr abundance in the layer is  $[\text{Pr}/\text{H}] \geq 4$ . Table 4 (column 10) presents the corresponding non-LTE equivalent widths of the  $\text{Pr II}$  and  $\text{Pr III}$  lines. For comparison, we give also the LTE equivalent widths, calculated with the obtained Pr distribution, and the non-LTE abundance corrections. It can be seen that net non-LTE correction to the Pr abundance  $\Delta_{\text{NLTE}}(\text{Pr II}) - \Delta_{\text{NLTE}}(\text{Pr III})$  is at the level of 1.8 dex, for the stratified atmosphere. In order to make the LTE element abundances from the lines of  $\text{Pr II}$  and  $\text{Pr III}$  consistent, the layer of enhanced praseodymium has to be located above the uppermost depth point in our model,  $\log \tau_{5000} = -8$  (!). This means that any stratification analysis for the praseodymium in roAp stars has to be performed based on non-LTE line formation. It is worth noting that a location of the enriched praseodymium layer turns out to be very similar to that found for the neodymium in our earlier study.

A quality of fitting the observed praseodymium lines in HD 24712 with the derived Pr stratification profile is illustrated in Fig. 9 and Fig. 10. The synthetic flux profiles are convolved with the instrumental profile (spectral resolution  $R = 80000$ ), projected rotational velocity  $v_e \sin i = 5.6 \text{ km s}^{-1}$  and additional broadening parameter equivalent to radial-tangential profile of  $V_{\text{mac}} = 4 \text{ km s}^{-1}$  for the  $\text{Pr II}$  and  $6 \text{ km s}^{-1}$  for the  $\text{Pr III}$  lines. One cannot expect to get the same quality fits for the magnetic star with a complex chemically stratified atmosphere as those for the Sun. Nevertheless, our non-LTE stratification analysis allows to reproduce reasonably well the observed  $\text{Pr II}$  and  $\text{Pr III}$  lines in HD 24712, contrary to the case of the uniform distribution of Pr. In the latter case, we can fit the  $\text{Pr III}$  5300Å and 6195Å profiles (dashed curves in Fig. 10) with the Pr abundance determined from non-LTE analysis of the  $\text{Pr III}$  lines only,  $\log(\text{Pr}/\text{H}) = -7.32$ , but calculate extremely strong lines of  $\text{Pr II}$  compared to the observations.

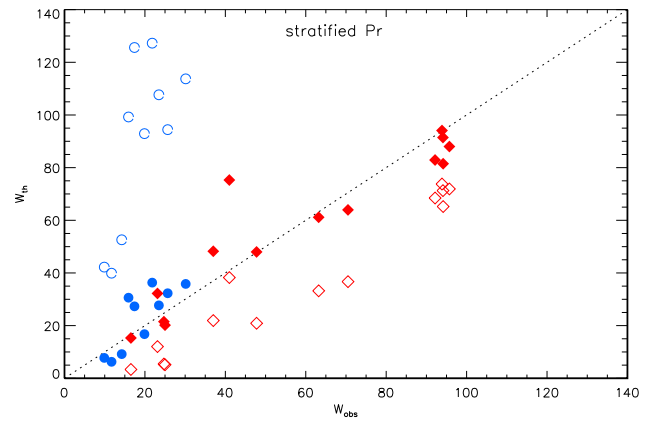


**Fig. 9.** Observed equivalent widths of the  $\text{Pr II}$  (circles) and  $\text{Pr III}$  (diamonds) lines in HD 24712 compared with the theoretical non-LTE (filled symbols) and LTE (open symbols) equivalent widths for the stratified Pr distribution shown in the top panel of Fig. 7 by continuous line.

The knowledge of the Pr abundance distribution is important for a study of atmospheric pulsations. Fig. 11 shows a distribution of the pulsation RV amplitudes and phases of the Pr lines as well as of the lines of  $\text{Nd II}$  and  $\text{Nd III}$  and of the  $\text{H}\alpha$  core in the atmosphere of HD 24712. The RV data are taken from Ryabchikova et al. (2007b, Online Table 4). We use the average optical depths of line formation which are calculated with the element abundance distributions obtained in this study for the Pr and by Mashonkina et al. (2005) for the Nd. We follow the formalism suggested by Achmad et al. (1991) with using the contribution function to the emergent line radiation. The computed values  $\log \tau_{5000}^l$  are given in Table 4 (column 12). For comparison, we present there (column 13) also the average optical depths of line formation based on the contribution function to the emergent total (line + continuum) radiation,  $\log \tau_{5000}^{l+c}$ . It was emphasized by Achmad et al. that the first approach provides more realistic depth of line formation, in particular, for weak lines, for which the continuum contribution shifts an average depth formation downward. This effect becomes much more important for the case of stratified atmosphere. When the contribution function to the total radiation is used, the formation depth of most  $\text{Pr II}$  lines is shifted well below the enhanced Pr abundance layer. The non-LTE formation depths for the  $\text{H}\alpha$  core have been computed according to Mashonkina et al. (2008). It can be seen from Fig. 11, that with the stratified Pr and Nd abundance distributions found based on non-LTE line formation, we get a consistent picture typical for running pulsation wave where the amplitudes and phases grow towards upper layers. A gap of  $\sim 0.5$  dex at  $\log \tau_{5000} \sim -4.5$  may be caused by the uncertainties of the modelling.

### 6.3. The uncertainties of Pr stratification analysis

In this subsection, we discuss the effects due to the uncertainties of atomic parameters and due to ignoring magnetic intensification of spectral lines.

**Photoionization cross-sections.** The statistical equilibrium of  $\text{Pr II/III}$  in the stratified atmosphere is mainly defined by enhanced photoionization of  $\text{Pr II}$ . We perform test calculations using various photoionization cross-sections. When the hydroge-

**Table 4.** Equivalent widths (in mÅ) of the Pr II and Pr III lines observed in HD 24712 (column 4) and calculated using non-LTE and LTE approach for the model 7250/4.3/0 with the homogeneous (columns 6 - 8) and stratified (columns 9 - 11) element distributions.

| $\lambda$ ,<br>Å | $E_{low}$ ,<br>eV | $\log gf$          | $W_{obs}$<br>mÅ | $V_{mic}$ ,<br>km s <sup>-1</sup> | [Pr/H] = 3 |            |                 | Stratified distribution* |            |                 |                           |                          |
|------------------|-------------------|--------------------|-----------------|-----------------------------------|------------|------------|-----------------|--------------------------|------------|-----------------|---------------------------|--------------------------|
|                  |                   |                    |                 |                                   | $W_{LTE}$  | $W_{NLTE}$ | $\Delta_{NLTE}$ | $W_{LTE}$                | $W_{NLTE}$ | $\Delta_{NLTE}$ | $\log \tau_{5000}^{NLTE}$ | $\log \tau_{5000}^{I+c}$ |
| 1                | 2                 | 3                  | 4               | 5                                 | 6          | 7          | 8               | 9                        | 10         | 11              | 12                        | 13                       |
| <b>Pr II</b>     |                   |                    |                 |                                   |            |            |                 |                          |            |                 |                           |                          |
| 5002.44          | 0.80              | -0.87 <sup>1</sup> | 12              | 1.0                               | 31         | 30         | 0.02            | 40                       | 6          | 1.12            | -4.50                     | -0.65                    |
| 5110.76          | 1.15              | 0.32 <sup>2</sup>  | 30              | 1.0                               | 95         | 96         | -0.02           | 114                      | 36         | 1.11            | -4.57                     | -1.86                    |
| 5129.54          | 0.65              | -0.13 <sup>1</sup> | 26              | 1.0                               | 77         | 78         | -0.03           | 94                       | 32         | 1.17            | -4.68                     | -2.08                    |
| 5135.14          | 0.95              | 0.01 <sup>3</sup>  | 16              | 1.0                               | 80         | 80         | -0.01           | 99                       | 31         | 1.07            | -4.59                     | -1.47                    |
| 5292.62          | 0.65              | -0.26 <sup>3</sup> | 23              | 1.0                               | 84         | 84         | 0.00            | 108                      | 28         | 1.19            | -4.60                     | -1.64                    |
| 5322.77          | 0.48              | -0.32 <sup>3</sup> | 22              | 1.0                               | 99         | 100        | -0.01           | 127                      | 36         | 1.18            | -4.64                     | -1.44                    |
| 5681.88          | 1.16              | -0.60 <sup>2</sup> | 10              | 1.0                               | 34         | 33         | 0.02            | 42                       | 8          | 1.02            | -4.49                     | -0.75                    |
| 6017.80          | 1.11              | -0.26 <sup>2</sup> | 20              | 1.0                               | 69         | 70         | -0.02           | 93                       | 17         | 1.10            | -4.48                     | -1.03                    |
| 6165.94          | 0.92              | -0.20 <sup>2</sup> | 17              | 1.0                               | 92         | 93         | -0.02           | 126                      | 27         | 1.13            | -4.55                     | -1.38                    |
| 6656.83          | 1.82              | 0.08 <sup>2</sup>  | 14              | 1.0                               | 41         | 39         | 0.03            | 53                       | 9          | 1.06            | -4.47                     | -1.19                    |
| <b>Pr III</b>    |                   |                    |                 |                                   |            |            |                 |                          |            |                 |                           |                          |
| 4910.82          | 0.17              | -1.95 <sup>4</sup> | 37              | 1.7                               | 10         | 17         | -0.29           | 22                       | 48         | -0.51           | -5.20                     | -2.65                    |
| 4929.12          | 0.36              | -2.07              | 23              | 1.0                               | 6          | 11         | -0.27           | 12                       | 32         | -0.61           | -5.17                     | -2.06                    |
| 5284.69          | 0.17              | -0.77              | 92              | 1.0                               | 48         | 60         | -0.36           | 68                       | 83         | -0.48           | -6.31                     | -5.74                    |
| 5299.99          | 0.36              | -0.72              | 94              | 1.05                              | 44         | 58         | -0.36           | 65                       | 81         | -0.48           | -6.24                     | -5.66                    |
| 5844.41          | 1.24              | -1.01              | 48              | 1.0                               | 13         | 20         | -0.24           | 21                       | 48         | -0.62           | -5.45                     | -4.02                    |
| 5998.97          | 0.17              | -1.87              | 63              | 1.55                              | 14         | 24         | -0.29           | 33                       | 61         | -0.45           | -5.47                     | -3.81                    |
| 6053.00          | 0.00              | -1.98              | 70              | 1.55                              | 14         | 24         | -0.29           | 37                       | 64         | -0.42           | -5.44                     | -3.92                    |
| 6090.01          | 0.36              | -0.87              | 94              | 1.1                               | 46         | 61         | -0.36           | 71                       | 91         | -0.53           | -6.19                     | -5.58                    |
| 6160.23          | 0.17              | -1.02              | 96              | 1.1                               | 43         | 59         | -0.37           | 72                       | 88         | -0.43           | -6.23                     | -5.69                    |
| 6195.62          | 0.00              | -1.07              | 94              | 1.0                               | 46         | 63         | -0.40           | 74                       | 94         | -0.57           | -6.19                     | -5.63                    |
| 6500.04          | 1.72              | -1.26              | 25              | 1.0                               | 3          | 5          | -0.26           | 5                        | 22         | -0.70           | -5.11                     | -2.13                    |
| 6616.46          | 1.55              | -1.50              | 25              | 1.0                               | 3          | 5          | -0.25           | 5                        | 20         | -0.69           | -5.07                     | -1.92                    |
| 6692.25          | 1.16              | -2.11              | 17              | 1.0                               | 2          | 3          | -0.27           | 3                        | 15         | -0.73           | -5.02                     | -1.14                    |
| 6706.70          | 0.55              | -1.49              | 41              | 1.5                               | 18         | 30         | -0.31           | 38                       | 75         | -0.58           | -5.49                     | -4.22                    |

<sup>1</sup> Li et al. (2007); <sup>2</sup> Kurucz & Bell (1995); <sup>3</sup> Ivarsson et al. (2001); <sup>4</sup> this study, for all Pr III lines,

\* It is shown in the bottom panel of Fig. 7 by continuous curve.

nous photoionization cross-sections are increased by a factor of 30 the overionization of Pr II is amplified and  $\Delta_{NLTE}$  increases by 0.03 dex to 0.05 dex for different Pr II lines. The uncertainty of photoionization cross-sections is much less important for Pr III. Reducing the hydrogenous photoionization cross-sections by a factor of 100 has much larger effect on both the Pr II and Pr III lines. In this case, the layer of enhanced Pr has to be shifted outward by  $\Delta \log \tau_{5000} \approx 0.5$  to agree the abundances of Pr from two ionization stages. The obtained Pr abundance distribution is shown by dashed curve in the top panel of Fig. 7. We emphasize that even with the lowest photoionization cross-sections the ionization equilibrium Pr II/Pr III deviates significantly from the TE one and non-LTE removes approximately 1.5 dex of the difference between the Pr abundances derived from the Pr II and Pr III lines under the LTE assumption. As was discussed in our earlier paper (Mashonkina et al. 2005), the adopted hydrogenic approximation gives, probably, the low limit for the photoionization cross-sections for the levels in the rare-earth elements. So, we under- rather than overestimate non-LTE effects for Pr II/III in our calculations.

**Collision rates.** In SE computations, we assume an effective collision strength to be equal  $\Upsilon = 1$  for every forbidden transition. This may be incorrect. The  $R$ -matrix method calculations for electron impact excitation in Ca II (Meléndez et al. 2007) show that  $\Upsilon$  depends on the transition energy separation. For example, at electron temperatures we are concerned with,  $\Upsilon > 30$  for the forbidden transitions with  $\Delta E_{ij} < 0.1$  eV, while

$\Upsilon \leq 0.1$  if  $\Delta E_{ij} > 10$  eV. For the fine-structure transitions in Fe II, the  $R$ -matrix method predictions of Ramsbottom et al. (2007) give  $\Upsilon \geq 5$ . We perform non-LTE calculations for Pr II/III assuming that for the forbidden transitions,  $\Upsilon$  depends on the transition energy separation as follows:  $\log \Upsilon = 1.5$  for  $\Delta E_{ij} < 0.1$  eV,  $\log \Upsilon = -0.38\Delta E_{ij} + 1.54$  for  $\Delta E_{ij} = 0.1$  eV – 4 eV,  $\log \Upsilon = -0.17\Delta E_{ij} + 0.67$  for  $\Delta E_{ij} = 4$  eV – 10 eV, and  $\log \Upsilon = -1$  for  $\Delta E_{ij} \geq 10$  eV. These approximations are based on an extensive set of the data of Meléndez et al. (2007) for the forbidden transitions in Ca II. With stronger collisional coupling the low-excitation levels to the Pr II ground state the departures from LTE are weakened for the Pr II transitions arising from the levels with  $E_{exc} < 0.8$  eV, and they are strengthened for the remaining transitions in Pr II and for all transitions in Pr III. The Pr abundance distribution obtained from these test calculations is shown by dotted curve in the top panel of Fig. 7. We find that no revision is required outside  $\log \tau_{5000} = -6.5$  and inside  $\log \tau_{5000} = -4$  compared to the distribution found in Sect. 6.2, while the praseodymium abundance is decreased by up to 0.2 dex in between.

**Magnetic field.** The magnetic field effects are taken into account in this study approximately by introducing a pseudo-microturbulence. First, this works only for strong spectral lines. Second, magnetic field and microturbulence affect the saturated line profile in different ways. Magnetic field splits the line into the Zeeman components making the line less deep (magnetic desaturation) and broader, while microturbulence does not affect

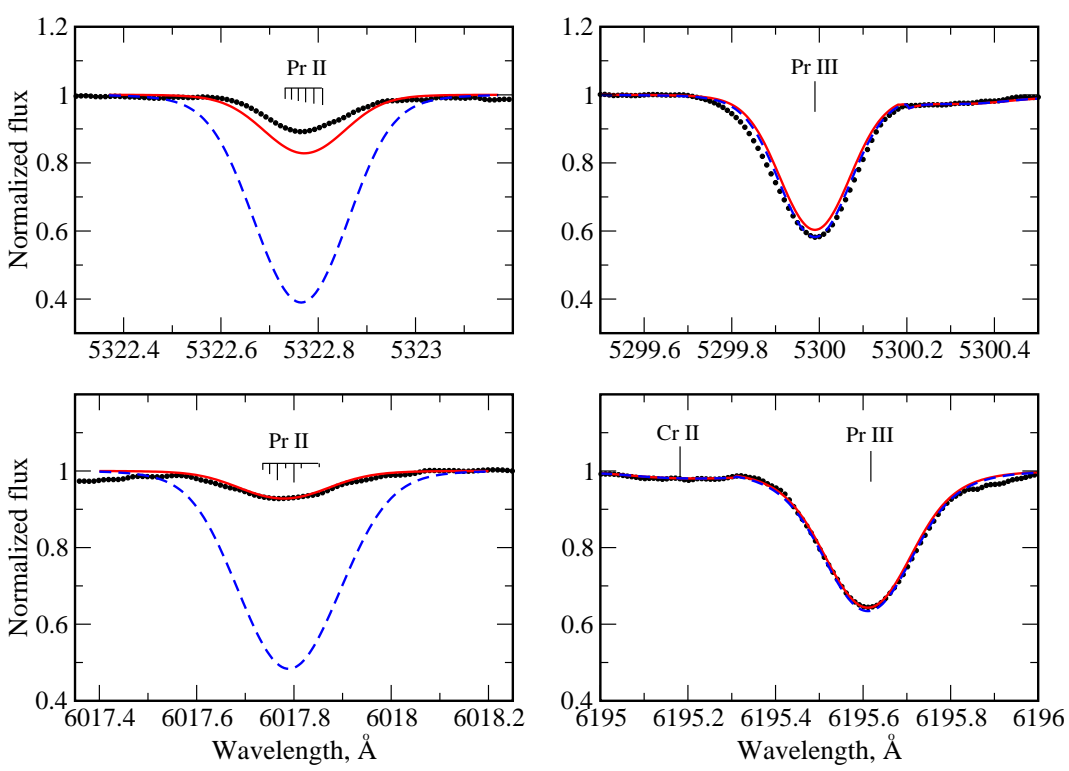


**Fig. 10.** A comparison between the observed (bold dots) and non-LTE spectra for the selected Pr II and Pr III lines in HD 24712. The non-LTE profiles from calculations with the derived Pr distribution are shown by continuous curves. Dashed curves correspond to the non-LTE profiles from calculations with  $\log(\text{Pr}/\text{H}) = -7.32$  everywhere in the atmosphere.

the line depth, but increases the half-width of the line profile. As was shown in Sect. 6.1, taking into account Zeeman splitting produces small changes, by 0.16 dex, on average, in the derived Pr abundances compared to those determined without magnetic field. Such an effect cannot influence our conclusion on stratified distribution of Pr in the atmosphere of HD 24712. Zeeman splitting may also result in different line formation depths compared to that for turbulently broadened lines and, therefore, in a different location of the Pr enriched layer. We estimate this effect using the strongest Pr III  $\lambda 5300\text{\AA}$  line. Zeeman splitting of this line is represented by the three components. From comparison of the computed single line with  $V_{\text{mic}} = 1.05 \text{ km s}^{-1}$  with the triplet with zero microturbulence we deduce that the magnetic desaturation may lead to only a 0.2 dex decrease of the Pr abundance in the layer and in the shift of Pr abundance profile downward, by 0.35 dex in  $\log \tau_{5000}$  scale.

Thus, the uncertainty of the used atomic data on photoionization cross-sections and electron impact excitation cross-sections and ignoring the magnetic field in non-LTE analysis cannot change our conclusion as regards an existence of inhomogeneous distribution of Pr in the atmosphere of HD 24712.

## 7. Conclusions

In this study, we first presented a comprehensive model atom for Pr II/III based on the measured and the calculated energy levels. Non-LTE line formation for an extended list of Pr II and Pr III lines was considered for the Sun and for the temperatures characteristic of A type stars,  $T_{\text{eff}} = 7250 \text{ K} - 9500 \text{ K}$ . At  $T_{\text{eff}} \leq 8000 \text{ K}$ , Pr II represents the majority of the element and the departures from LTE for the Pr II lines are small. They are mainly caused by a deviation of the line source function from the Planck

function and may result in the non-LTE abundance corrections of different sign for various lines. Overionization of Pr II at  $T_{\text{eff}} \geq 8500 \text{ K}$  leads to depleted total absorption in the Pr II lines and positive  $\Delta_{\text{NLTE}}$  that grows with temperature. Non-LTE leads to strengthening the Pr III lines and negative abundance corrections over the whole range of stellar parameters. As Pr III becomes the majority species,  $\Delta_{\text{NLTE}}$  of the Pr III lines decreases in absolute value.

Using the modern laboratory data for oscillator strengths of the Pr II lines, improved partition function of Pr II based on the laboratory and the calculated energy levels, we determine the non-LTE abundance of praseodymium in the solar atmosphere,  $\log(\text{Pr}/\text{H})_{\odot} = -11.15 \pm 0.08$  and  $\log(\text{Pr}/\text{H})_{\odot} = -11.10 \pm 0.08$ , for the ATLAS9 and the Holweger & Müller (1974) models, respectively. The Pr abundance based on the theoretical model is 0.05 dex to 0.10 dex larger compared to the meteoritic value recommended by Grevesse et al. (1996), Palme & Jones (2005), Lodders (2003), or Asplund et al. (2005), but the deviation is still within the error bars.

For the roAp star HD 24712, the element abundances from two ionization stages, Pr II and Pr III, reveal a discrepancy of two orders of magnitude if the atmosphere is assumed to be chemically homogeneous. Neither non-LTE, nor magnetic effects can be responsible for such abundance anomaly.

Introducing the layer with a strongly enhanced Pr abundance in the outer atmosphere provides a natural possibility to describe the lines of both ionization stages, Pr II and Pr III, for the single element distribution. We find that the required Pr overabundance in the layer is  $[\text{Pr}/\text{H}] \geq 4$  at  $\log \tau_{5000} < -4$ . The obtained praseodymium and neodymium stratifications provide a possibility to explain the distributions of the pulsational characteristics (radial velocity amplitudes and phases) over the significant

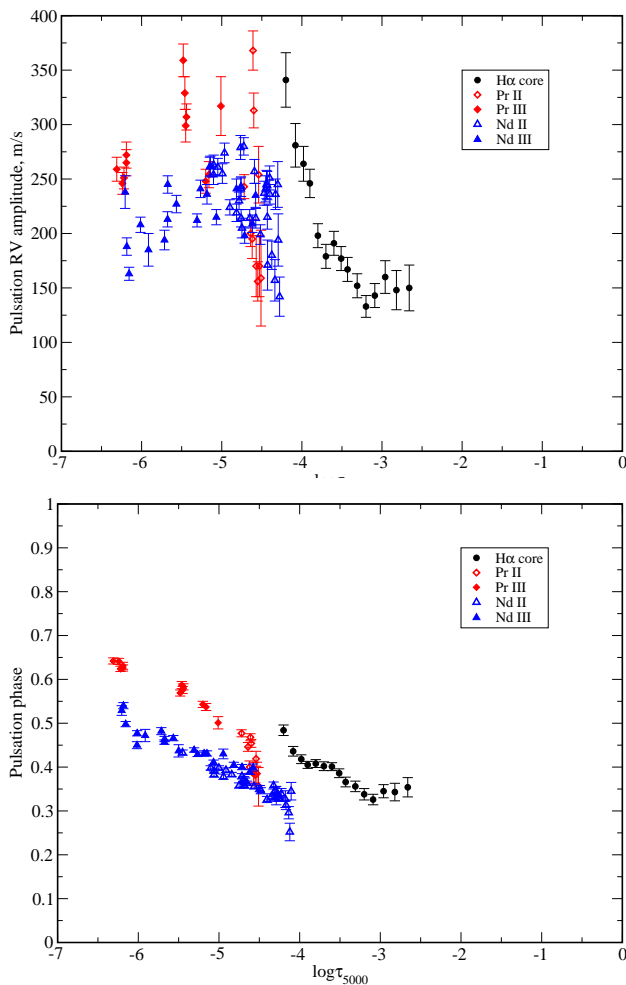


**Fig. 11.** Pulsation radial velocity amplitude (top panel) and phase (bottom panel) variations for the lines of Pr II (open diamonds), Pr III (filled diamonds), Nd II (open triangles), Nd III (filled triangles), and the  $H\alpha$  core (filled circles) as a function of the optical depth in the atmosphere of the roAp star HD 24712 with the stratified distribution of Pr and Nd.

part of the atmosphere of HD 24712, where the lines of these elements as well as the core of the  $H\alpha$  line are formed.

Similar abundance profiles found empirically for the Nd (Mashonkina et al. 2005) and the Pr in the atmosphere of HD 24712 point to some common physical mechanisms producing accumulation of these two elements in the uppermost atmospheric layers. The main mechanism can be radiatively driven diffusion. The theoretical diffusion calculations of LeBlanc & Monin (2004) for Cr and Fe and of Alecian & Stift (2007) for Mg, Si, Ca, Ti, Fe predict the existence of the abundance jumps up to several orders of magnitude in stable stellar atmospheres with effective temperatures characteristic of Ap stars. Similar abundance profiles are derived empirically for these elements in the atmospheres of roAp stars (Ryabchikova 2008). Opposite to REEs, Mg to Fe are accumulated in the lower atmosphere. Due to difficulties with the atomic data no diffusion calculations have been performed for the REEs to check the validity of the empirical distributions, but this situation is improving and we hope to see first REE diffusion calculations in the future.

We are planning to extend non-LTE line formation study to other REE which reveal a discrepancy between the element

abundances derived from the lines of two ionization stages in the roAp stars. As was shown for Nd by Mashonkina et al. (2005) and for Pr in the present work, the departures from LTE for the lines of the first and the second ions are of the opposite sign, and they are large if the element is concentrated in the uppermost atmospheric layers where collisions are inefficient to establish thermodynamic equilibrium. In such a case, a stratification analysis for REE has to be performed based on non-LTE line formation.

**Acknowledgements.** The authors are grateful to J.-F. Wyart for help in calculations of Pr II and Pr III spectra. This research was supported by the Russian Foundation for Basic Research with grant 08-02-00469-a, by the Presidium RAS Programme “Origin and evolution of stars and galaxies”, and by the Leading Scientific School grant 4224.2008.2. TR also acknowledges a partial support from the Austrian Science Fund (FWF-P17580N2).

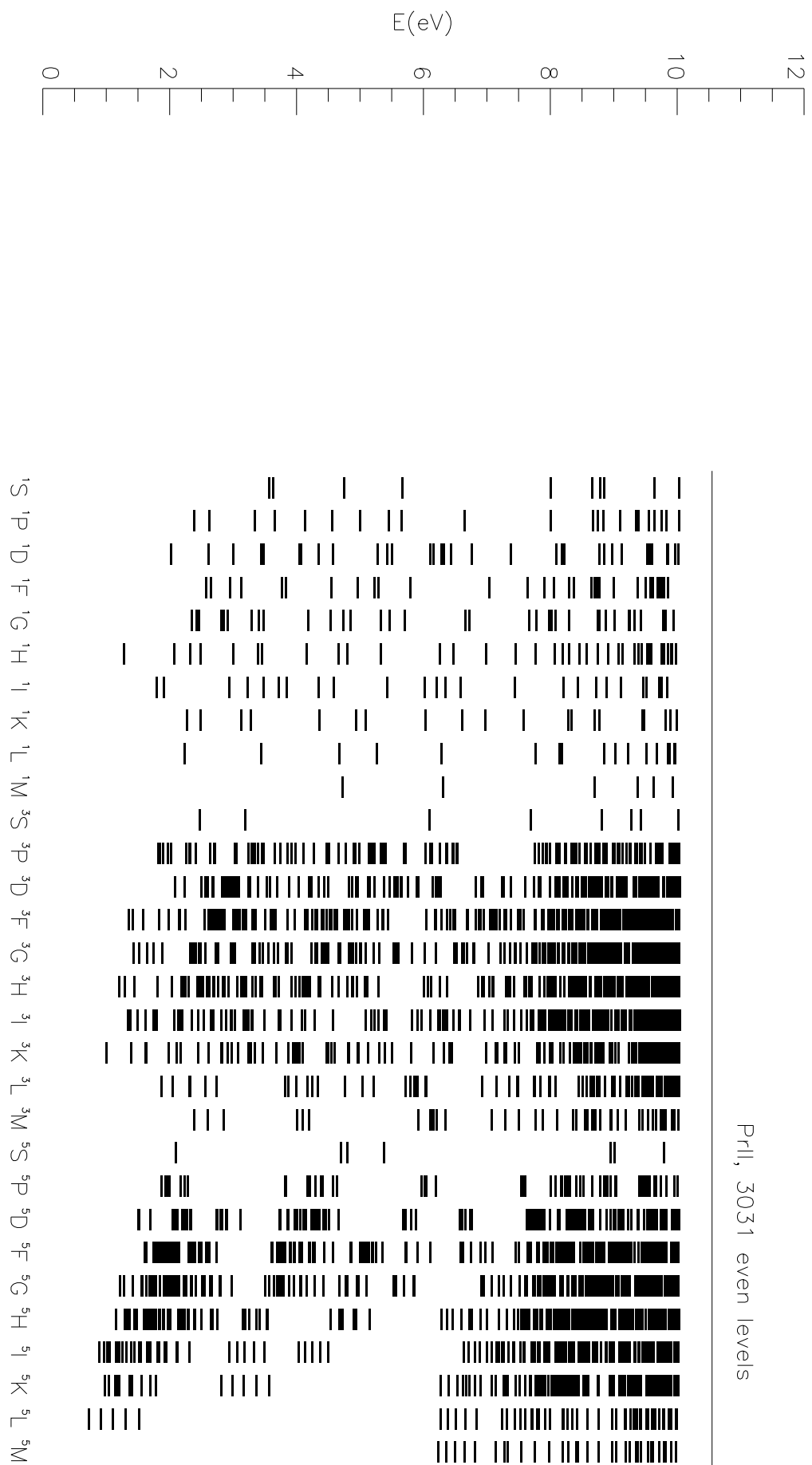
## References

- Achmad, I., de Jager, C., & Nieuwenhuijzen, H. 1991, *A&A*, 250, 445  
 Alecian, G. & Stift, M. J. 2007, *A&A*, 475, 659  
 Allard, N. F., Drira, I., Gerbaldi, M., et al. 1998, *A&A*, 335, 1124  
 Anders, E., Grevesse, N. 1989, *Geoch. & Cosmochim. Acta* 53, 197  
 Anstee, S.D. & O'Mara, B.J. 1995, *MNRAS*, 276, 859  
 Asplund, M., Grevesse, N., & Sauval, A.J. 2005, *ASP Conf. Ser.*, 336, 25  
 Bard, A., Kock, A., & Kock, M. 1991, *A&A*, 248, 315  
 Biémont, E., Grevesse, N., & Hauge, Ø. 1979, *Solar Phys.*, 61, 17  
 Biémont, E., Garnir, H.P., Palmeri, P., et al. 2001, *Phys. Rev.*, A64, 2503  
 Biémont, E., Lefebvre, P.H., Quinet, P., et al. 2003, *European Phys. J.*, D27, 33  
 Brewer, L. 1971, *JOSA*, 61, 1666  
 Butler K., & Giddings J. 1985, *Newsletter on the analysis of astronomical spectra* No. 9, University of London  
 Canuto, V. M., Goldman, I., & Mazzitelli, I. 1996, *ApJ*, 473, 550  
 Castelli, F. & Kurucz, R. 2001, *A&A*, 372, 260  
 Cowan, R.D. 1981, *The Theory of Atomic Structure and Spectra*, Univ. of California Press. Berkeley, California. USA  
 Cowley, C.R. & Bord, D.J. 1998, in *The scientific impact of the Goddard High Resolution Spectrograph*. *ASP Conf. Ser.* 143, 346  
 Cowley, C.R., Ryabchikova, T., Kupka, F., et al. 2000, *MNRAS*, 317, 299  
 Drawin, H.-W. 1961, *Z. Physik* 164, 513  
 Fuhrmann, K., Pfeiffer, M., Frank, C., et al. 1997, *A&A*, 323, 909  
 Furman, B., Stefanska, D., Stachowska, E., et al. 2001, *European Phys. J.* D17, 275  
 Gelbmann, M., Ryabchikova, T.A., Weiss, W.W., et al. 2000, *A&A*, 356, 200  
 Ginibre, A. 1989a, *Physica Scripta*, 39, 694  
 Ginibre, A. 1989b, *Physica Scripta*, 39, 710  
 Ginibre, A. 1990, *Atomic Data and Nuclear Data Tables*, 44, 1  
 Grevesse, N., Noels, A., & Sauval, A.J. 1996, *ASP Conf. Ser.*, 99, 117  
 Grupp, F. 2004, *A&A*, 420, 289  
 Heiter, U., Kupka, F., van 't Veer-Menneret, C., et al. 2002, *A&A*, 392, 619  
 Holweger, H., & Müller, E.A. 1974, *Solar Phys.*, 39, 19  
 Ivarsson, S., Litzén, U., & Wahlgren, G. 2001, *Phys. Scr.*, 64, 455  
 Ivarsson, S., Wahlgren, G., & Ludwig, H.-G. 2003, *BAAS*, 35, 1421  
 Kato, K. 2003, *PASJ*, 55, 1133  
 Kochukhov, O. 2003, *A&A*, 404, 669  
 Kochukhov, O. 2007, in *Physics of Magnetic Stars*, eds. I.I. Romanyuk and D. O. Kudryavtsev, Nizhnij Arkhyz, p. 109  
 Kochukhov, O., Khan, S., & Shulyak, D. 2005, *A&A*, 433, 671  
 Kupka, F., Piskunov, N., Ryabchikova, T.A., et al. 1999, *A&AS* 138, 119  
 Kurucz, R. L. 1994a, *Opacities for Stellar Atmospheres*. CD-ROM No. 2-8. Cambridge, Mass  
 Kurucz, R. L. 1994b, *SYNTHES Spectrum Synthesis Programs and Line Data*. CD-ROM No. 18. Cambridge, Mass  
 Kurucz, R. L. & Bell, B. 1995, *Atomic Line Data*. Kurucz CD-ROM No. 23. Cambridge, Mass  
 Kurucz, R. L., Furenlid, I., Brault, J., & Testerman, L. 1984, *NSO Atlas No. 1: Solar Flux Atlas from 296 to 1300 nm*, Sunspot, NSO  
 Lage, C.S. & Whaling, W. 1976, *JQSRT*, 16, 537  
 LeBlanc, F. & Monin, D. 2004, *The A-Star Puzzle*, IAU 224, eds. J. Zverko, W.W. Weiss, J. Žižňovský & S.J. Adelman, 193  
 Li, R., Chatelain, R., Holt, R.A., et al. 2007, *Phys. Scr.*, 76, 577  
 Lodders, K. 2003, *ApJ*, 591, 1220  
 Martin, W.C., Zalubas, R., & Hagan, L. 1978, *Atomic energy levels - The Rare Earth Elements*. NSRDS-NBS 60, U.S. Gov. Print. Off., Washington. 1978.

- Mashonkina, L. 2008, in Non-LTE line formation for trace elements in stellar atmospheres, Eds. R. Monier, B. Smalley, Ph. Stee, and G. Wahlgren, EAS Publ. Ser (in press)
- Mashonkina, L., Ryabchikova, T.A., & Ryabtsev, A.N. 2005, A&A, 441, 309
- Mashonkina, L., Zhao, G., Gehren, T. et al. 2008, A&A, 478, 529
- Meggers, W.F, Corliss, C.H., & Scribner, B.F. 1975, NBS Monograph 145, U.S. Gov. Print. Off., Washington, D.C.
- Meléndez, M., Bautista, M.A., & Badnell, N.R. 2007, A&A, 469, 1203
- Palme, H., & Jones, A. 2005, in Meteorites, Comets and Planets: Treatise on Geochemistry, vol. 1. Ed. A. M. Davis, Elsevier Publ., Amsterdam, The Netherlands, 41
- Palmeri, P., Quinet, P., Fremat, Y., et al. 2000, ApJS, 129, 367
- Ramsbottom, C. A., Hudson, C. E., Norrington, P. H., & Scott, M. P. 2007, A&A, 475, 765
- Reetz, J. K. 1991, Diploma Thesis, Universität München
- Ryabchikova, T. 2008, Contr. Astron. Obs. Skalnaté Pleso, 38, 257
- Ryabchikova, T.A., Kochukhov, O., & Bagnulo, S. 2008, A&A, 480, 811
- Ryabchikova, T.A., Landstreet J.D., Gelbmann M.J., et al. 1997, A&A, 327, 1137
- Ryabchikova, T., Nesvacil, N., Weiss, W.W., et al. 2004, A&A, 423, 705
- Ryabchikova, T., Piskunov, N., Kochukhov, O., et al. 2002, A&A, 384, 545
- Ryabchikova, T., Ryabtsev, A., Kochukhov, O., & Bagnulo, S. 2006, A&A, 456, 329
- Ryabchikova, T., Sachkov, M., Kochukhov, O., & Lyashko, D. 2007a, A&A, 473, 907
- Ryabchikova, T., Sachkov, M., Weiss, W.W., et al. 2007b, A&A, 462, 1103
- Ryabchikova, T.A., Savanov, I.S., Hatzes, A.P., et al. 2000, A&A, 357, 981
- Ryabchikova, T.A., Savanov, I.S., Malanushenko, V.P., & Kudryavtsev, D.O. 2001, Astron. Rep., 45, 382
- Rybicki, G.B., & Hummer, D.G. 1991, A&A, 245, 171
- Rybicki, G.B., & Hummer, D.G. 1992, A&A, 262, 209
- Scholl T., Holt R., Masterman D., et al. 2002, Can.J.Phys., 80, 713
- Smith, W.W. & Gallagher, A. 1966, Phys. Rev., 145, 26
- Steenbock, W. & Holweger, H. 1984, A&A, 130, 319
- Takeda, Y. 1994, PASJ, 46, 53
- van Regemorter, H. 1962, ApJ, 136, 906
- Wickliffe, M. E., Lawler, J. E., & Nave, G. 2000, JQSRT, 66, 363



# Online Material



Pr II, 3031 even levels

**Fig. 1.** The Pr II even term structure.

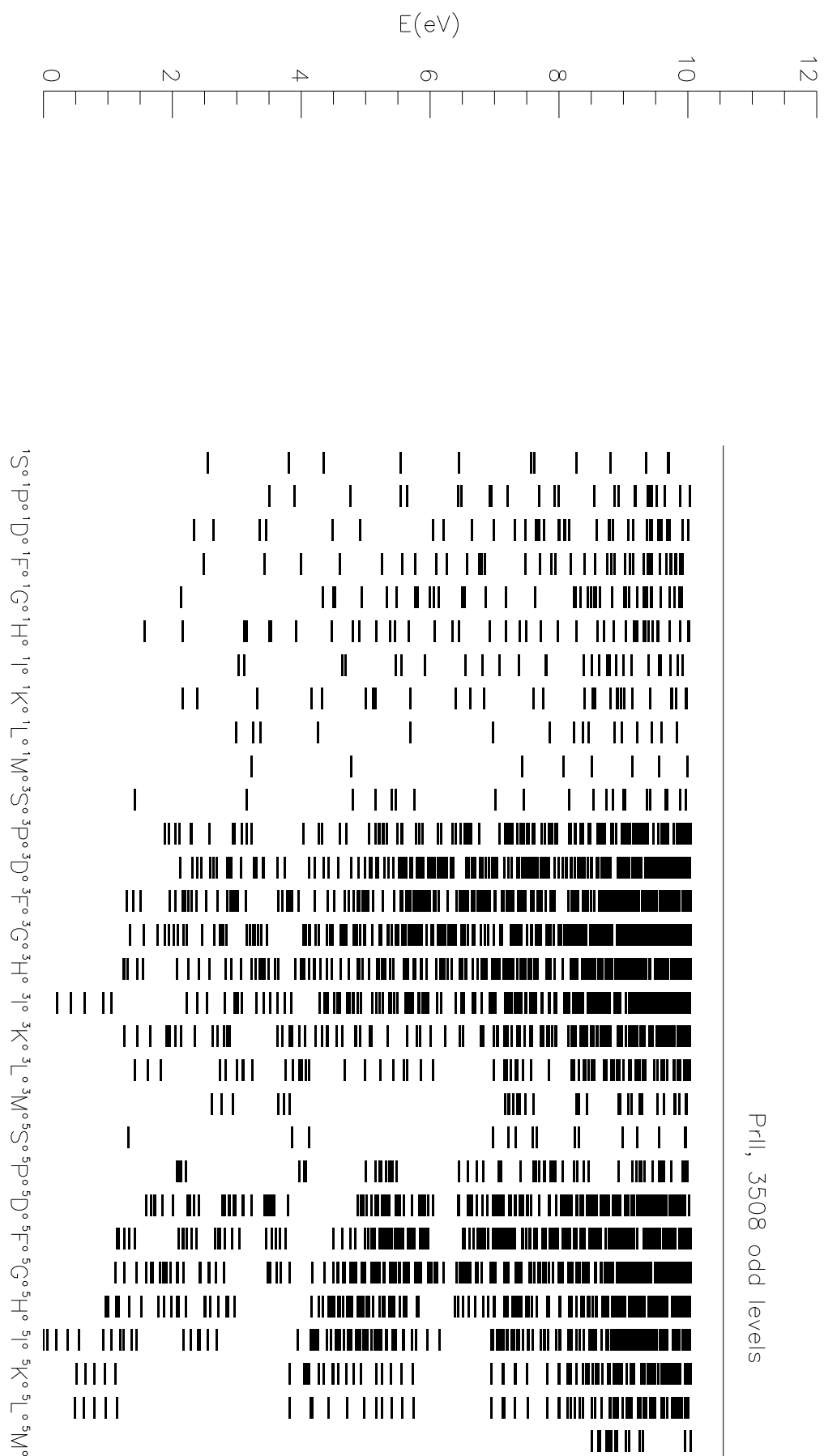


**Fig.2.** The Pr II odd term structure.

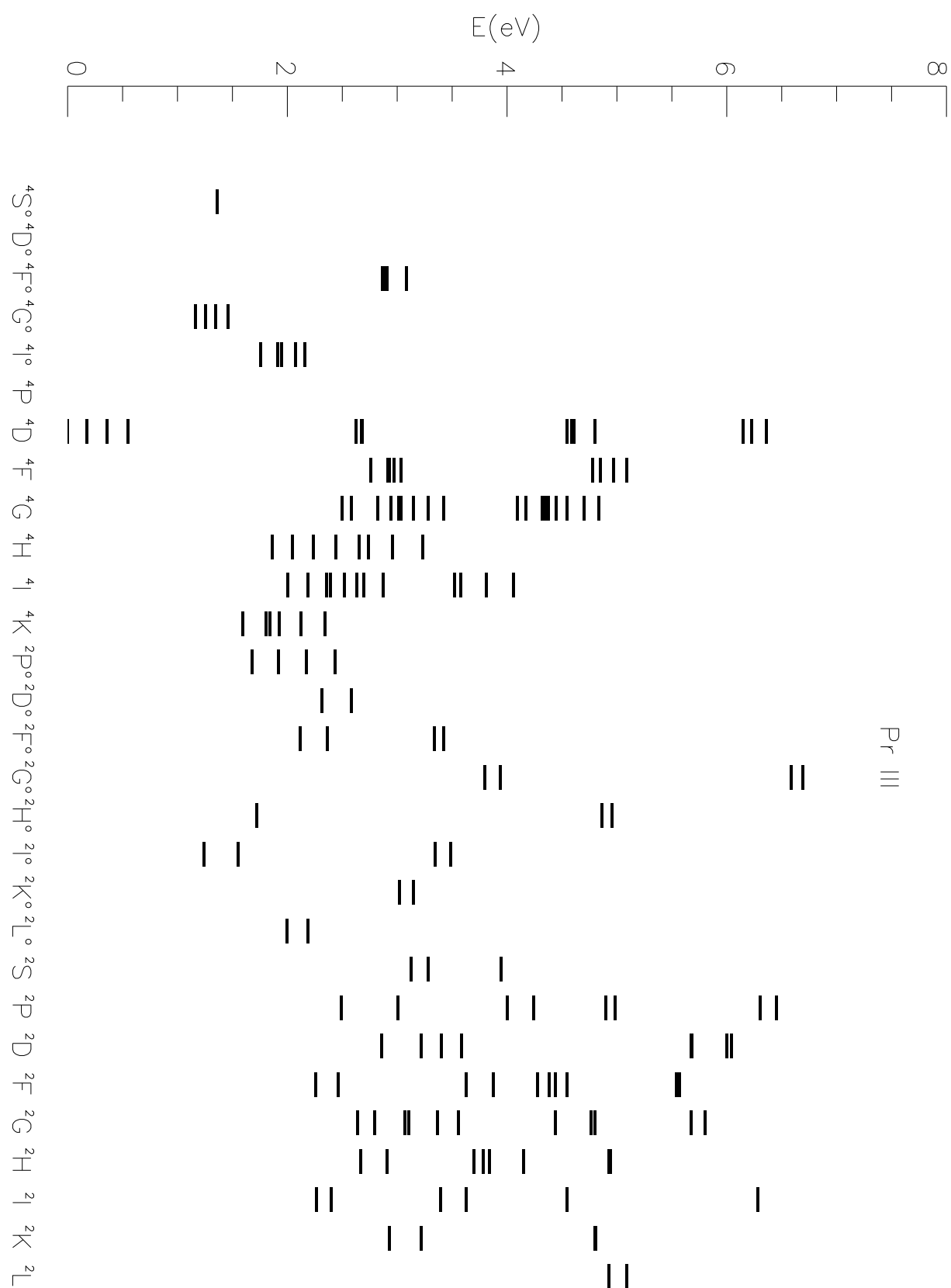


**Fig. 3.** The Pr III model atom.